JOURNAL OF GEOPHYSICAL RESEARCH, VOL. 111, D12213, doi:10.1029/2005JD006575, 2006

Click Here for Full Article

Dust model intercomparison (DMIP) study over Asia: Overview

I. Uno,[1] Z. Wang,[2] M. Chiba,[3] Y. S. Chun,[4] S. L. Gong,[5] Y. Hara,[1] E. Jung,[6,7] S.-S. Lee,[4] M. Liu,[8] M. Mikami,[3] S. Music,[9,10] S. Nickovic,[9,10] S. Satake,[11] Y. Shao,[6] Z. Song,[12] N. Sugimoto,[13] T. Tanaka,[3] and D. L. Westphal[8]

Received 8 August 2005; revised 16 February 2006; accepted 21 March 2006; published 28 June 2006.

[1] An intercomparison study involving eight dust emission/transport models over Asia (DMIP) has been completed. Participating dust models utilize a variety of dust emission schemes, horizontal and vertical resolutions, numerical methods, and different meteorological models. Two huge dust episodes occurred in spring 2002 and were used for the DMIP study. Meteorological parameters, dust emission flux and dust concentration (diameter < 20 μm) are compared within the same domain on the basis of PM and NIES lidar measurements. We found that modeled dust concentrations between the 25% and 75% percentiles generally agreed with the PM observations. The model results correctly captured the major dust onset and cessation timing at each observation site. However, the maximum concentration of each model was 2–4 times different. Dust emission fluxes from the Taklimakan Desert and Mongolia differ immensely among the models, indicating that the dust source allocation scheme over these regions differs greatly among the various modeling groups. This suggests the measurements of dust flux and accurate updated land use information are important to improve the models over these regions. The dust vertical concentration profile at Beijing, China, and Nagasaki, Japan, has a large scatter (more than two times different) among the models. For Beijing, the scaled dust profile has a quite similar vertical profile and shows relatively good agreement with the lidar extinction profile. However, for Nagasaki, the scaled dust profiles do not agree. These results indicate that modeling of dust transport and removal processes between China and Japan is another important issue in improving dust modeling.

Citation: Uno, I., et al. (2006), Dust model intercomparison (DMIP) study over Asia: Overview, *J. Geophys. Res.*, *111*, D12213, doi:10.1029/2005JD006575.

1. Introduction

[2] Dust emission and transport modeling plays an important role in understanding the recent increase of Asian dust episodes. From the late 1990s, dust models have been developed at universities, research institutes, and government agencies, and then applied to the Asian region [e.g., *Wang et al.*, 2000; *Park and In*, 2003; *Gong et al.*, 2003; *Liu et al.*, 2003; *Shao et al.*, 2003; *Uno et al.*, 2001, 2003]. These models have reproduced many important observational facts and retrieved valuable information to elucidate characteristics of Asian dust phenomena. Recently, the Asia Pacific Regional Aerosol Characterization Experiment (ACE-Asia) [*Huebert et al.*, 2003] provided an excellent opportunity to examine a large-scale Asian dust episode using numerical dust transport models [e.g., *Gong et al.*, 2003; *Liu et al.*, 2003; *Chin et al.*, 2003; *Uno et al.*, 2004]. At least three regional dust models were applied for the ACE-Asia periods and reported reasonable simulated results. However, their estimated dust emission amounts ranged widely from 105 Tg/(2 months), 250 Tg/(3 months) to 640 Tg/(16 days). Similar scatter in the dust emission flux results is also evident in the modeling results from *Park and In* [2003] and *Shao et al.* [2002]. Moreover, dust transport patterns from the emission source region are usually very similar, but the predicted surface level concentration sometimes shows a difference of more than two orders of magnitude. Such wide scattering of the estimated dust emission and concentration reflects differences in dust

[1]Research Institute for Applied Mechanics, Kyushu University, Fukuoka, Japan.
[2]Institute of Atmospheric Physics, Chinese Academy of Sciences, Beijing, China.
[3]Meteorological Research Institute, Tsukuba, Japan.
[4]Meteorological Research Institute, Korean Meteorological Administration, Seoul, Korea.
[5]Meteorological Service of Canada, Toronto, Ontario, Canada.
[6]Department of Physics and Materials Science, City University of Hong Kong, Kowloon, Hong Kong.
[7]Now at Center for Atmospheric Sciences, Scripps Institution of Oceanography, University of California, San Diego, La Jolla, USA.
[8]Naval Research Laboratory, Monterey, California, USA.
[9]Euro-Mediterranean Centre on Insular Coastal Dynamics, University of Malta, Foundation for International Studies, Valletta, Malta.
[10]Now at Environment Division, Atmospheric Research and Environment Program, World Meteorological Organization, Geneva, Switzerland.
[11]Research Institute for Humanity and Nature, Kyoto, Japan.
[12]National Meteorological Centre, China Meteorological Administration, Beijing, China.
[13]National Institute for Environmental Studies, Tsukuba, Japan.

Copyright 2006 by the American Geophysical Union.
0148-0227/06/2005JD006575$09.00

Table 1. Description of DMIP Model Group

	University/Institute							
	Naval Research Laboratory, Monterey, USA	Korean METRI, Korea	MSC, Canada	iCOD/DREAM Malta	Hong Kong City University, China	Kyushu University, Japan	Naval Research Laboratory, Monterey, USA	MRI-JMA, Japan
Dust model	COAMPS	ADAM	NARCM	DREAM	CEMSYS5	CFORS	NAAPS	MASINGAR
Meteorological database or global model name	COAMPS (with NOGAPS for boundary and initial)	RDAPS (Regional Data-Assimilation and Prediction System/KMA)	RCM (Canadian Regional Climate Model with NCEP data)	NCEP/Eta (with NCEP data)	T213 forecast or NCEP reanalysis and CEMSYS4	RAMS (with ECMWF)	NOGAPS (global model)	MRI/JMA 98 GCM (with JMA GANAL)
Model domain (horizontal and vertical information)	Lambert projection (center 42°N, 106°E); horizontal 27km (with 301 × 221 grids), vertically 46 layers (up to 32 km)	Lambert conformal projection (center 38°N, 128°E); horizontal 30 km (with 191 × 171 grids), vertically 25 layer (up to 18 km)	north polar stereographic projection (center 35.6°N, 106.6°E) with a horizontal resolution of 45 km at 60°N (160 × 110 grids), vertically 22 layers (up to 30 km)	rotated lat-lon (center 39°N, 112.5°E) horizontal 0.5° (with 67 × 81 grids), vertically 23 layers (up to 16 km)	Lambert projection: horizontal 50 km, vertically 25 layers	rotated polar-stereographics (center 25°N, 115°E) horizontal 80 km (with 100 × 90 grids), vertically 23 layer (up to 23 km)	latitude-longitude grid; 1° horizontal resolution; 24 levels between surface and 100 mb	global; horizontal about 125 km (with 320 × 160 grids); vertically 20 layers (up to 45 hPa)
Thickness of first layer, m	10	39	45	86	100	72	20	40
Dust emission: threshold velocity or friction velocity	Ustar[4] [*Nickling and Gillies*, 1993]	Ustar[4] [*Westphal et al.*, 1988] + modified [*In and Park*, 2003]	Ustar[3] [*Marticorena and Bergametti*, 1995]	Ustar[3] [1-(ustar_t/ustar)^2] [*Shao et al.*, 1993]	*Shao* [2001]; u_t* is calculated by *Shao and Lu* [2000]	Ustar[4] [*Gillette and Passi*, 1988]	Ustar[4] [*Westphal et al.*, 1987, 1988]	*Shao et al.* [1996]; u*t is calculated by *Shao and Lu* [2000]
Dust size range (diameter)	0.05–36 μm	0.2–74 μm	0.1–40.96 μm	1.46–76 μm	continuous to any size, mostly up to 40 μm	0.2–40 μm	2 μm	0.2–20 μm
Dust size bins	10 bins	11 bins	12 bins	4 bins	any, usually 6 bins	12 bins	1 bin	10 bins
Dust density, kg/m^3	2600	2600	2650	2500–2650	2600	2520	2500	2650
Dust particle size distribution	bimodal lognormal size of sand-blasting model [*Alfaro et al.*, 1997]	log normal distribution	linearly with respect to a cutoff of size (radius < 0.25 μm and >16 μm) and to log radius between 0.25 and 16 μm	discrete diameters: 1.46, 12.2, 36, 76 μm	2, 11, 22, 52, 90, 125 μm	linearly with respect to radius (r < 1 μm) and to log radius (r > 1 μm)	none	determined by the dust emission model and parent soil particle size distribution
Snow cover	USGS land use 1-km database	not included	function of observed monthly averaged snow cover fraction (1°)	not considered	not considered	function of observed monthly averaged snow cover fraction (1°)	forecasted by NOGAPS	output of the land surface model (SiB)

Table 1. (continued)

	University/Institute							
	Naval Research Laboratory, Monterey, USA	Korean METRI, Korea	MSC, Canada	iCOD/DREAM Malta	Hong Kong City University, China	Kyushu University, Japan	Naval Research Laboratory, Monterey, USA	MRI-JMA, Japan
Land use data	USGS land use 1-km database	USGS vegetation data (1 km resolution)	USGS vegetation data (1 km resolution) and Chinese Desertification Map [*Chinese Academy of Sciences*, 1998]	USGS vegetation data (1 km resolution)	merged USGS and LREIS soil data	USGS vegetation data (1 km resolution)	USGS vegetation data (1 km resolution)	*DeFries and Townshend* [1994] (1° resolution)
Soil texture information	N/A[a]	*Park and In* [2003], *In and Park* [2003]	Chinese soil texture map and FAO soil texture data outside China	FAO soil texture data	USDA soil texture classification; minimally and fully dispersed particle size analysis	FAO soil texture data	none	*Webb et al.* [2000] (1° resolution)
Roughness length	USGS land use 1-km database	*Park and In* [2003], *In and Park* [2003]	calculation of the roughness length from density and height of the roughness elements [*Pielke*, 1984; *Marticorena et al.*, 1997]	predefined NCEP/ETA model	substrate roughness length and estimation from NDVI	RAMS LEAF2	internal database based on USGS 1-km database, with seasonal variation	SiB defaults
Total dust emission (period A), Tg	101	(57.4)[b]	106	167	336	26.7	22.8[c]	78
Total dust emission (period B), Tg	103	(47.0)[b]	21.6	218	215	26.7	18.1[c]	42
References	*Liu et al.* [2003]	*In and Park* [2003], *Park and In* [2003]	*Gong et al.* [2003]	*Nickovic et al.* [2001]	*Shao et al.* [1993, 1996], *Shao* [2001]	*Uno et al.* [2003]	*Christensen* [1997]	*Tanaka and Chiba* [2005]

[a]N/A, not applicable.
[b]It does not include the Taklimakan Desert.
[c]Considers only those particles with diameters less than 10 microns.

Table 2. Required Model Output for Dust Model Intercomparison

Variable	Contents	Unit
DFLX	dust emission flux (d < 20 μm)	$mg/m^2/h$
DC1B	dust concentration at first model level (d < 20 μm)	$\mu g/m^3$
DC7H	dust concentration at 700 hPa (d < 20 μm)	$\mu g/m^3$
DCLN	dust column loading (height z < 10 km) (d < 20 μm)	mg/m^2
WS10	wind speed at 10 m level	m/s
USTR	surface friction velocity	m/s
USTH	threshold surface friction for dust lift up	m/s
PREP	precipitation rate	mm/h
DDRY	dust dry deposition (d < 20 μm)	$mg/m^2/3$ h
DWET	dust wet deposition (d < 20 μm)	$mg/m^2/3$ h

emission schemes, surface boundary data (such as soil texture, soil wetness, land use data including a recent desertification information), and atmospheric models (meteorological and transport models). Consequently, more detailed studies are required to reduce uncertainties related to Asian dust emission, transport and removal. In addition, a common understanding of the performance and uncertainty of dust erosion and transport models in the Asian region has become essential for developing dust storm forecast capacities in the region. At the 2nd Aeolian Dust Experiment on Climate Impact (ADEC [*Mikami et al.*, 2002, 2006]) Workshop in Xi'an, China, January 2003, an urgent need for an intercomparison of recent dust models was discussed and an agreement was reached to pursue this activity. On the basis of this agreement, the dust model intercomparison (DMIP) activity over the Asia region was initiated as an activity of the ADEC project. This paper presents an outline of this DMIP project, an overview of its major findings, and its conclusions.

2. Framework of DMIP

[3] The DMIP project was designed to gain an understanding of dust model characteristics by intercomparing independent simulations made by each group. For the model intercomparison period, two major dust episodes were selected: period A, 15–25 March 2002 (ten days), and period B, 4–14 April 2002 (ten days) because of the very dense dust onsets observed over a wide area including China, Korea, and Japan [e.g., *Chun and Lim*, 2004; *Shao et al.*, 2003; *Sugimoto et al.*, 2003]. As shown later in section 4.2, the maximum TSP concentration in period A exceeded 12 mg/m^3 at Beijing, and 2 mg/m^3 at Seoul.

[4] The DMIP project accepted all original dust model results without specifying either model resolution or land use (desertification) information (i.e., each group can use their own land use category information for possible dust emission sources). Furthermore, we specified no meteorological model field (or driver), therefore allowing participants to use their own meteorological fields to execute dust simulation. Each group was compelled to use its own dust model and submitted a description of the model and dust concentration fields. Dust transport models were required to include the Gobi Desert and Mongolia. Preferably, they also included the Taklimakan Desert as a potential dust source region. The eastern boundary of all model domains was required to cover all areas of Japan. These relatively lax specifications were utilized in order to accommodate as many participants as possible to this project, which, however, necessitated a very careful scheme to perform intercomparison of model results.

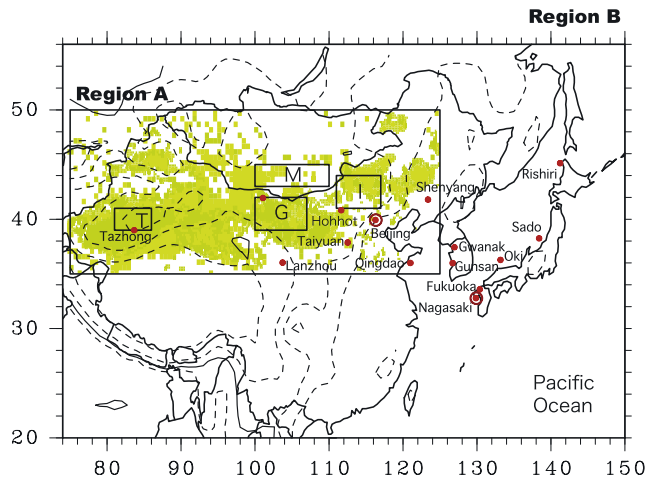

Figure 1. Model comparison of regions A and B. Square areas of T (Taklimakan; 81–86°E, 39–41°N), G (Gobi; 100–107°E, 39–42°N), M (Mongolia; 100–110°E, 43–45°N) and I (inner Mongolia; 111–117°E, 41–44°N) are used to produce averaged model statistics. Red dots show locations of model comparisons for wind speed and dust concentration. Double circles show locations of NIES lidar used in this paper.

[5] Nine dust modeling groups employed eight models in the DMIP project. Details of each dust model are summarized in Table 1. There were six regional dust models (horizontal resolutions of 27–80 km) and two global models (1° and 1.125°). In the vertical dimension, the resolution ranged from 20 to 46 levels. High-resolution models (horizontal grid size < 50 km) include the Coupled

Table 3. Geographical Locations of Selected Region and Stations

Region or Station	Longitude	Latitude	Elevation, m	Parameters
T	81–86°E	39–42°N	1250	meteorological and dust statistics
G	100–107°E	43–45°N	1425	meteorological and dust statistics
M	100–110°E	43–45°N	1346	meteorological and dust statistics
I	111–117°E	41–45°N	1206	meteorological and dust statistics
Beijing	116.46°E	39.92°N	55	WS, visibility, PM_{10}, TSP, lidar
Qingdao	120.30°E	36.1°N	77	dust
Seoul	126.90°E	37.50°N	49	dust
Fukuoka	130.40°E	33.60°N	12	dust
Nagasaki	129.80°E	32.78°N	30	lidar
Tazhong	83.67°E	39.00°N	1099	WS, visibility
Ejin Qi	101.07°E	41.95°N	941	WS, visibility
Lanzhou	103.73°E	36.03°N	1518	visibility, PM_{10}
Hohhot	111.65°E	40.82°N	1065	WS, visibility, PM_{10}
Taiyuan	112.53°E	37.87°N	780	WS, visibility, PM_{10}
Shenyang	123.38°E	41.8°N	45	visibility, PM_{10}
Gwanak–san	126.96°E	37.44°N	627	TSP
Gunsan	126.71°E	35.99°N	26	TSP
Oki	133.18°E	36.28°N	90	$PM_{2.5}$, PM_{10}
Sado	138.40°E	38.25°N	110	PM_{10}
Rishiri	141.23°E	45.12°N	40	$PM_{2.5}$, PM_{10}

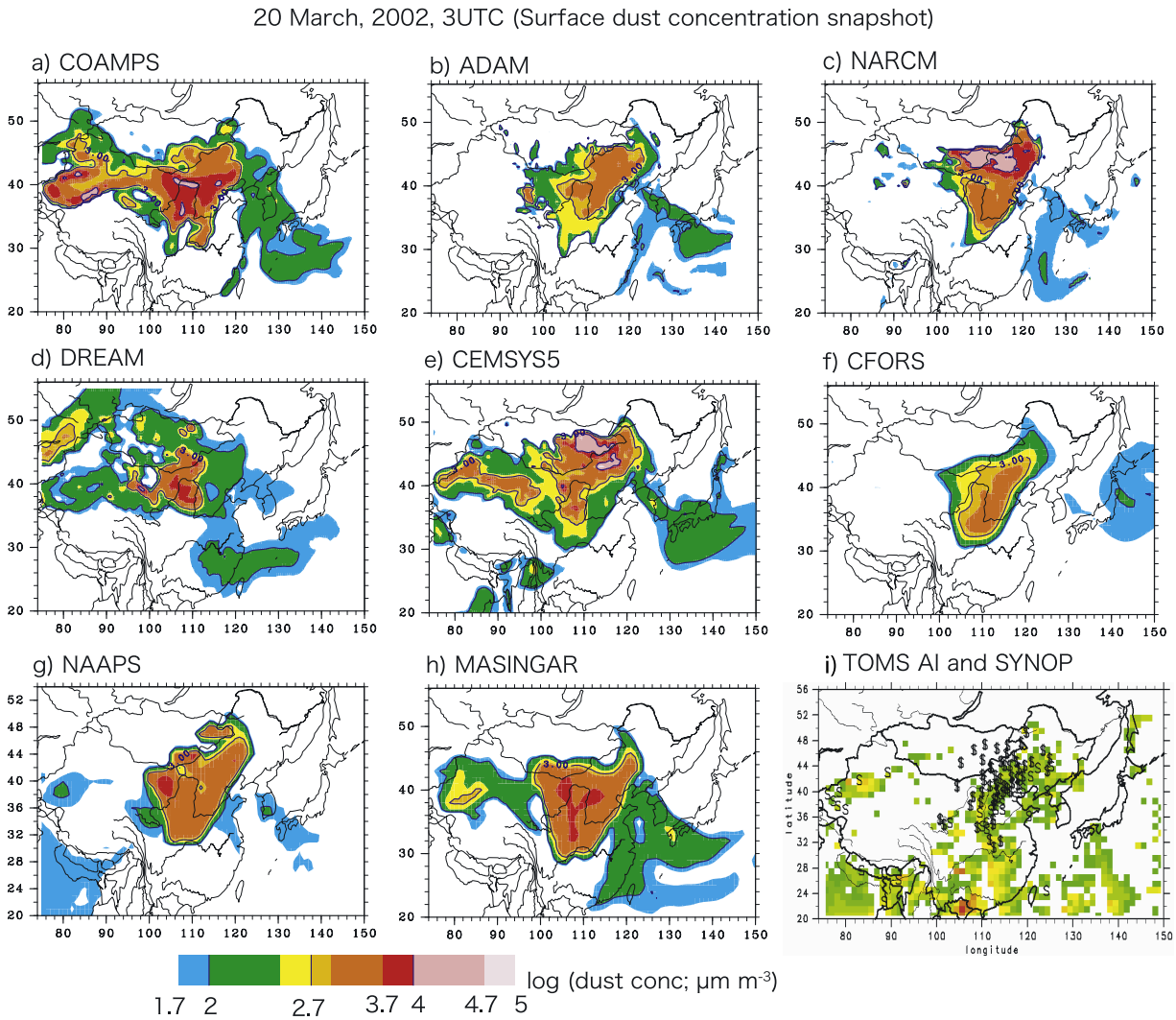

Figure 2. (a–h) Surface level dust concentration for each model at 20 March 2002 0300 UTC. Note that the color range of dust emission flux is logarithmic. (i) TOMS Aerosol Index (color) and individual SYNOP dust report (dollar signs) on that day.

Ocean/Atmospheric Mesoscale Prediction System (COAMPS [*Liu et al.*, 2003]), the Asian Dust Aerosol Model (ADAM [*Park and In*, 2003; *In and Park*, 2003]), the Dust Regional Atmospheric Model (DREAM [*Nickovic et al.*, 2001]), the Northern Aerosol Regional Climate Model (NARCM [*Gong et al.*, 2003]), and the Computational Environmental Modeling System version 5 (CEMSYS5 [*Shao et al.*, 2002]). Low-resolution model groups (horizontal grid size > 50 km) are the Chemical weather Forecasting model System (CFORS [*Uno et al.*, 2003]), the Navy Aerosol Analysis and Prediction System (NAAPS [*Christensen*, 1997; D. L. Westphal et al., Description of NAAPS: The Navy Aerosol Analysis and Prediction System, manuscript in preparation, 2006]), and Model of Aerosol Species in the Global Atmosphere (MASINGAR [*Tanaka and Chiba*, 2005]). A group from the Chinese Meteorological Agency (CMA) also submitted their results. Because their scheme and modeling concepts closely resemble those of the CEMSYS5 model, only the results from the CEMSYS5 model were shown in this paper.

[6] Most of regional models are using 1km resolution land use data set (shown in Table 1), and they are using a mosaic type subgrid treatment for dust emission. This is done by sorting land surface according to soil and vegetation data, and wind erosion model is then run for the land surface subgrid. The dust emission rate is then an area-weighted sum of the dust emission rate from the subcells. For global models such as MASINGAR, their grid size coincides with the resolution of land and soil texture information; no mosaic type approach is used (NAAPS is using the similar mosaic type treatment based on the USGS land use type).

[7] Except for the ADAM model, all model domains include the Taklimakan Desert area. Dust particle size ranges from 0.1 to 76 μm represented by a sectional approach of 1 to 12 bins. All dust emission schemes in DMIP are based on surface friction velocity (u_*), and most dust emission flux is calculated by a function of the third or fourth power of u_*. Three models (CEMSYS5, NARCM and MASINGAR) used the concept of saltation bombard-

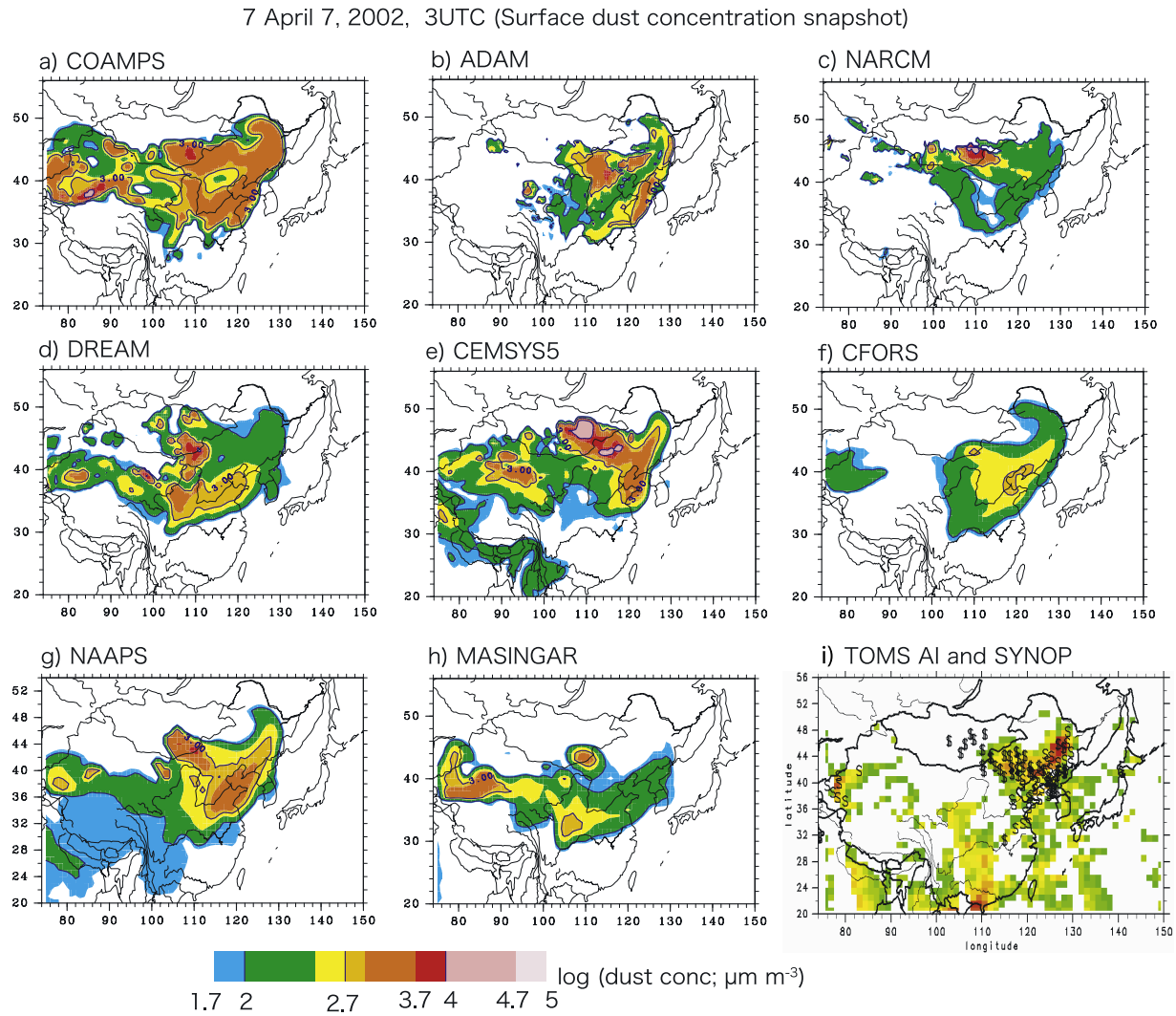

Figure 3. As in Figure 2 but for 3 April 2002 0300 UTC.

ment. One important point is that all dust models depend on regional or global meteorology models (e.g., NOGAPS, RDAPS, COAMPS, RCM, Eta, RAMS, and other AGCM, Table 1), which are based on objective analytical results from FNMOC, ECMWF, NCEP, JMA, KMA, etc. It is noteworthy that this DMIP project consists of various meteorological models, dust emission schemes, and land use information determined by each model development group and no adjustment is made to the submitted results from each model.

[8] Table 2 shows the required DMIP model outputs. Because of the differences in model horizontal resolution and map projection, the model data are interpolated to a 1° longitude-latitude grid, for the low-resolution group, and 0.5° for high-resolution group, at 3-hour intervals. Two examination regions were chosen for the model comparison (Figure 1): Region A covered the domain of 75–125°E and 35–50°N for analyses of detailed dust emission processes and concentration and region B covered the domain of 75–150°E and 20–55°N for analyses of transport processes and concentration.

[9] We required that the initial dust concentration be set to zero and allow no dust inflow from the lateral boundary because the comparison starting date for each period was selected as a dust storm free day. Some global models did not meet these conditions (such as NAAPS). Consequently, we generally analyzed the submitted model output from the second day of each period.

3. Observation Data

[10] The purpose of DMIP is not to score (rank) the model performances of each group. However, it is important to examine some model characteristics using observation data. The selected dust episodes were with huge and strong dust storms. Therefore we were able to access many important observation data such as the NIES Mie lidar network data (lidar observation networks at Beijing, Seoul, Nagasaki, and Tsukuba) [*Shimizu et al.*, 2004], WMO SYNOP report dust information (visibility and current weather report), and wind speed observations. Several surface measurements of Total Suspended Particle (TSP), PM_{10} and $PM_{2.5}$ data in China, Korea, and Japan were also available for DMIP.

[11] Figure 1 shows the location of observation sites, study regions A and B, and topography. Shaded areas

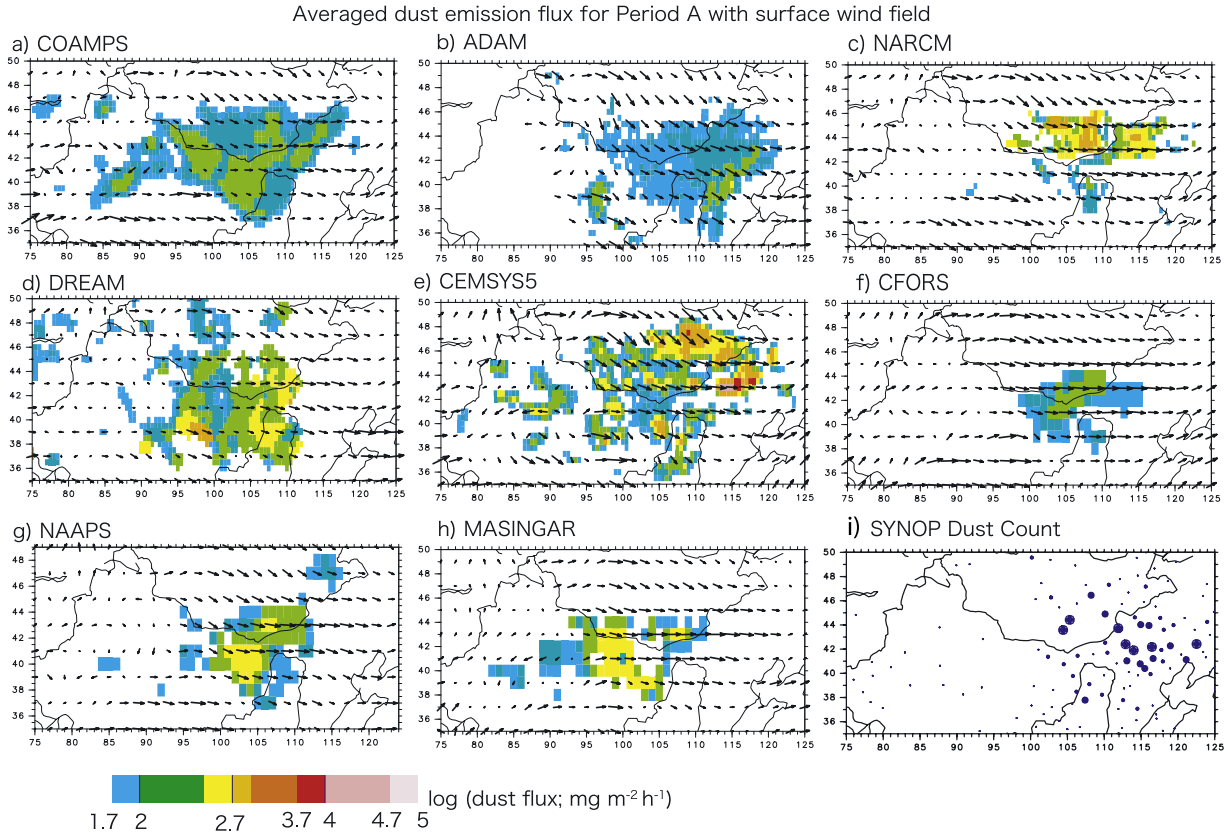

Figure 4. (a–h) Averaged dust emission flux for each model DFLX for period A (March 2002). Note that the color range of dust emission flux is logarithmic. (i) Total number of SYNOP dust weather events (current weather codes of 7–9 and 30–35) during each period (size of circle indicates the total number of events). Table 1 also shows the total dust emission flux during these two periods.

indicate potential dust emission sources (pure desert, loess, and advancing desertification area), as reported by *Gong et al.* [2003] and desert and semidesert areas, as reported in the USGS (United States Geological Survey) land use data set. The square boxes marked T (Taklimakan), G (Gobi), M (Mongolia), and I (inner Mongolia, China) are typical desert regions used for the detailed model comparisons in section 4.4. Please note that a specified area is a part of an important desert area but does not include the all region of traditional dust source area. The exact specifications of the regions and geographical locations of stations are described in Table 3.

[12] The SYNOP observations from Tazhong, Ejin Qi, Hohhot, Taiyuan, Shenyang, and Beijing were used for wind speed and dust concentration comparison. The SYNOP observation data were provided every 6 hours and wind speed was recorded with 1 m/s resolution. Note that the SYNOP site does not measure the dust concentration. However, *Shao et al.* [2003] found an empirical relationship between visibility and dust concentration by fitting the near-surface TSP observations to visibility as the following:

$$\begin{aligned} VC_{TSP} &= 3802.29\ D_V^{-0.85} && \text{for} \quad D_V < 3.5\ \text{km, and} \\ VC_{TSP} &= \exp(-0.11\ D_V + 7.62) && \text{for} \quad D_V > 3.5\ \text{km,} \end{aligned} \tag{1}$$

where VC_{TSP} is the dust concentration estimated by visibility in $\mu g/m^3$ and D_v is visibility in km. We used this estimated TSP concentration only when real TSP (or PM) data were unavailable.

[13] Daily averaged PM_{10} observations made by the State Environmental Protection Agency, China (SEPA) at Beijing, Taiyuan, Hohhot and Shenyang were also used. Beijing Normal University provides the TSP (hereafter BNU TSP) and PM_{10} for the March dust episodes [*Sun et al.*, 2004]. The Korea Meteorological Administration (KMA) provided 30 min interval TSP concentration at Gwanak-san and Gunsan. The East Asia Monitoring Network (EANET [*Network Center for EANET*, 2003]) provided hourly PM_{10} and $PM_{2.5}$ data for Oki, Sado, and Rishiri Islands.

[14] The National Institute for Environmental Studies (NIES) Mie lidar observation data from Beijing, China and Nagasaki, Japan [*Shimizu et al.*, 2004] were also used to compare vertical profiles of dust. This study used the dust extinction coefficient based on the lidar signal separated by a depolarization ratio. At Beijing, we also used time series data of the boundary layer averaged dust extinction coefficient for comparison.

4. Results and Discussion

4.1. Analyses of Dust Concentration, Wind Fields, and Dust Emission Flux

[15] Figures 2 and 3 show the instantaneous surface dust concentration in region B at the onset of both major dust

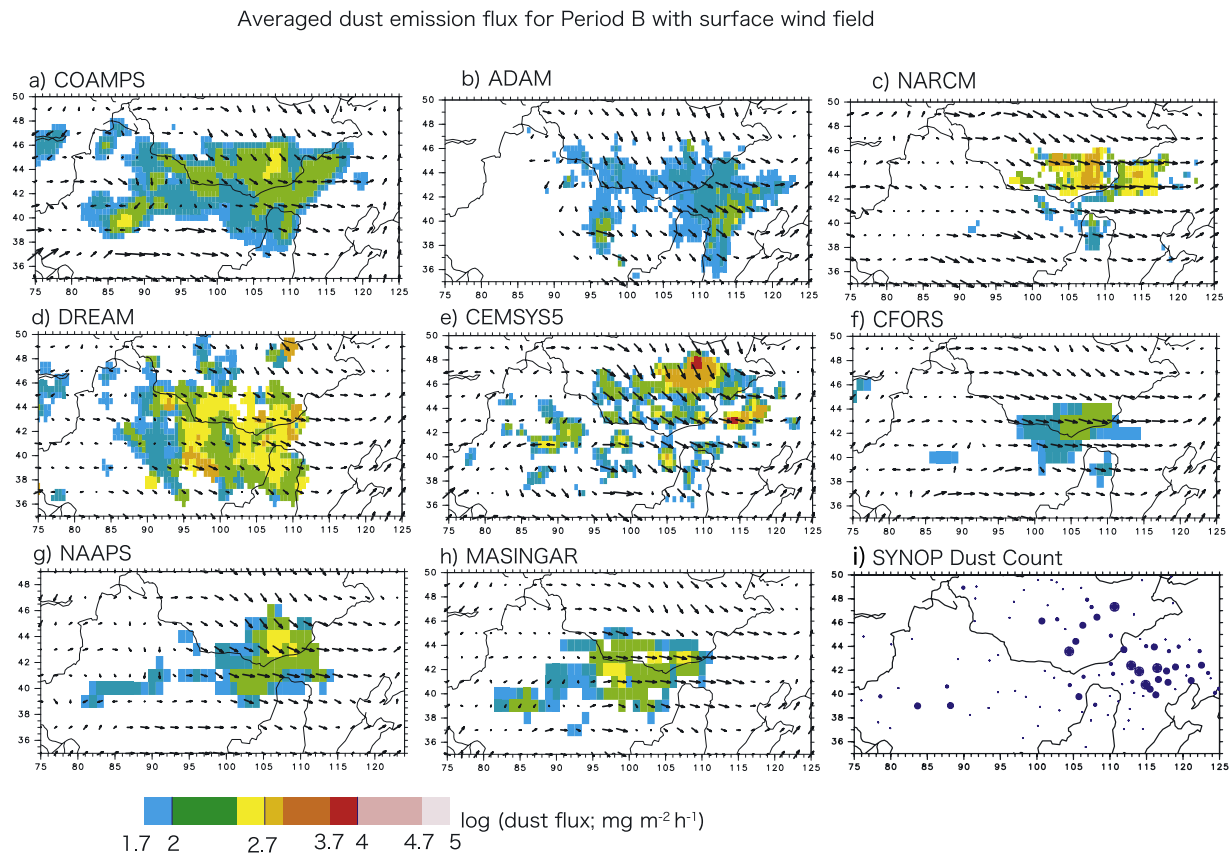

Figure 5. As in Figure 4 but for period B (April 2002).

storms. Distributions of the TOMS Aerosol Index (AI) and SYNOP dust reports are superimposed to allow comparison with the modeled dust distributions. Figures 2 and 3 clearly portray that the dust snapshot distribution appears quite similar in each model. Notwithstanding, the concentration levels are quite different. For example, the difference of dust concentration over the Beijing area on 20 March (Figure 2) is more than 10 times greater when comparing the minimum and maximum concentration models. Similar differences are apparent in the April dust snapshot (Figure 3). Results from low-resolution model groups generally produce smooth dust distributions, whereas high-resolution groups yield many patches of high dust-concentration regions. A great difference is evident in the dust concentrations over Mongolia and inner Mongolia: some models show dense dust concentrations.

[16] Figures 3 and 4 show an average of dust emission flux (DFLX, see Table 2) and wind fields for periods A and B. The averaged dust flux distributions indicate that the dust source region allocation differs greatly among modeling groups. For example, only two dust models allocate Mongolia and inner Mongolia region as high dust emission sources. Another area of large differences is the Taklimakan Desert. The total dust emission for region A (Table 1) ranged from 27 to 336 Tg, with a mean of 120 Tg for period A and 18 to 103 Tg, with a mean of 36.3 Tg for period B. Most models predicted less emission during period B than period A.

[17] The averaged 10-m wind field (Figures 4 and 5) shows fundamentally similar patterns. However, the wind flow over the Taklimakan area and Tibetan Plateau differ considerably between models. Some models indicate very calm conditions in the Taklimakan Desert, whereas other models give a systematic easterly wind. These differences in wind speed in the source regions partially account for the differences in the DFLX. There are small differences over the Beijing-Shandong peninsula region. Detailed analyses of wind speeds and other meteorological parameters are addressed in the following subsections.

4.2. Time Series Comparisons of Wind Field

[18] The time variation of the modeled 10-m wind speed and SYNOP observation is shown in Figure 6. Five SYNOP observation sites are selected for this time series comparison. To avoid an extreme value from some of the models, wind speeds from different models are sorted statistically and the minimum, quartile values (25%, 50% = mode and 75% percentile values), and maximum wind speed are shown in Figure 6. To measure the scatter from each model's results, we define the nondimensional scatter ratio S as

$$S_Q = (Q_{75\%} - Q_{25\%})/Q_{50\%}, \quad (2)$$

where $Q_{n\%}$ is the n% percentile value of the model variation of variable Q. In Figure 6, we also show the averaged value of S_{WS} and root-mean-square error (RMSE) for each site. Note that S = 1 means that a model variation range of $Q_{75\%}$ and $Q_{25\%}$ have the same value of mode ($Q_{50\%}$), which implies a large scatter of model output.

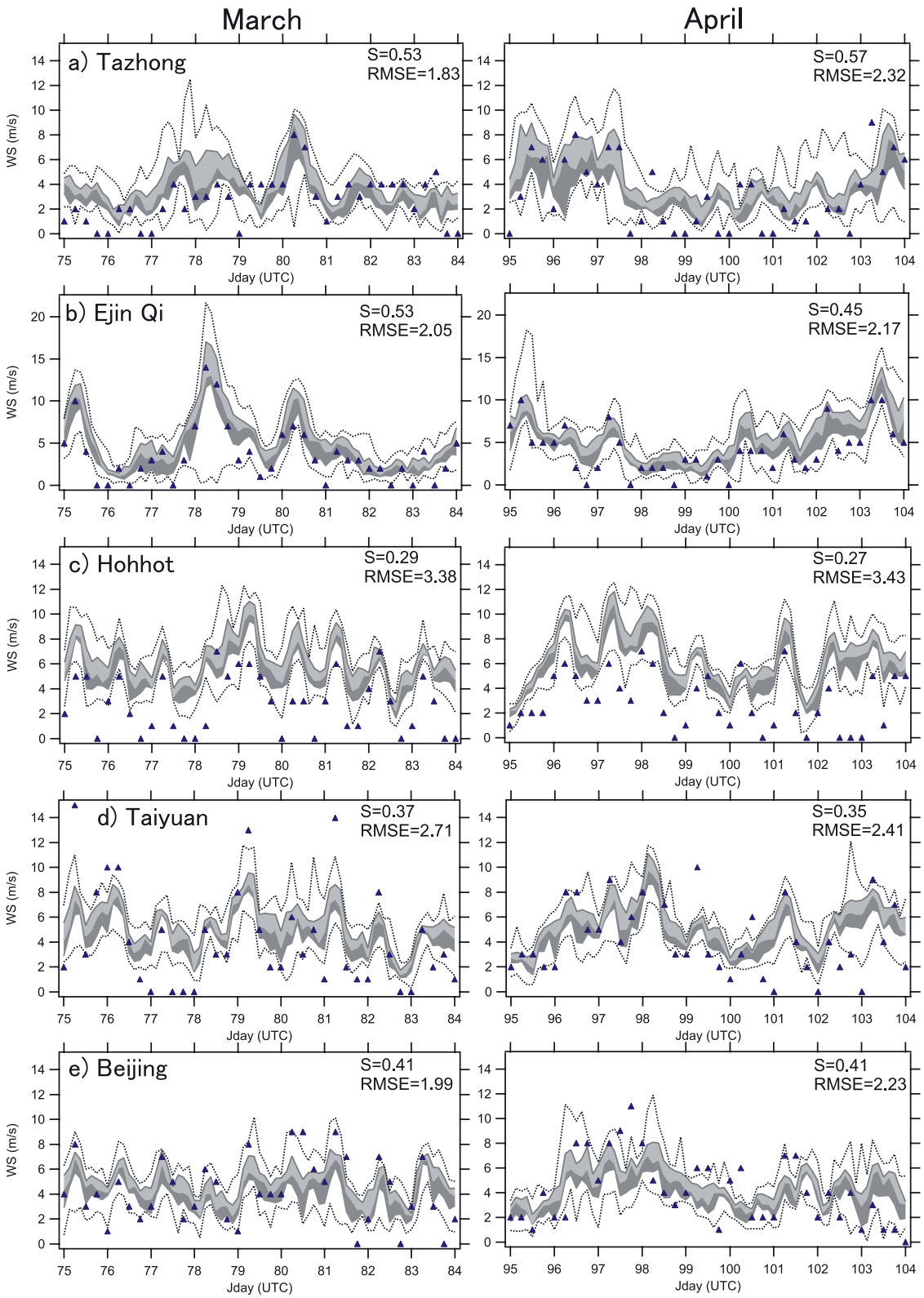

Figure 6. Time variation of wind speed at 10 m height (WS10). Sites are Tazhong, Ejin Qi, Hohhot, Taiyuan, and Beijing. WS_{10} from each model are shown by min, 25%, 50% (mode), 75%, and max values. Quartile values between the 25% and 75% percentiles are shaded. Triangles show the observed wind speed from SYNOP observation at 6-hour intervals.

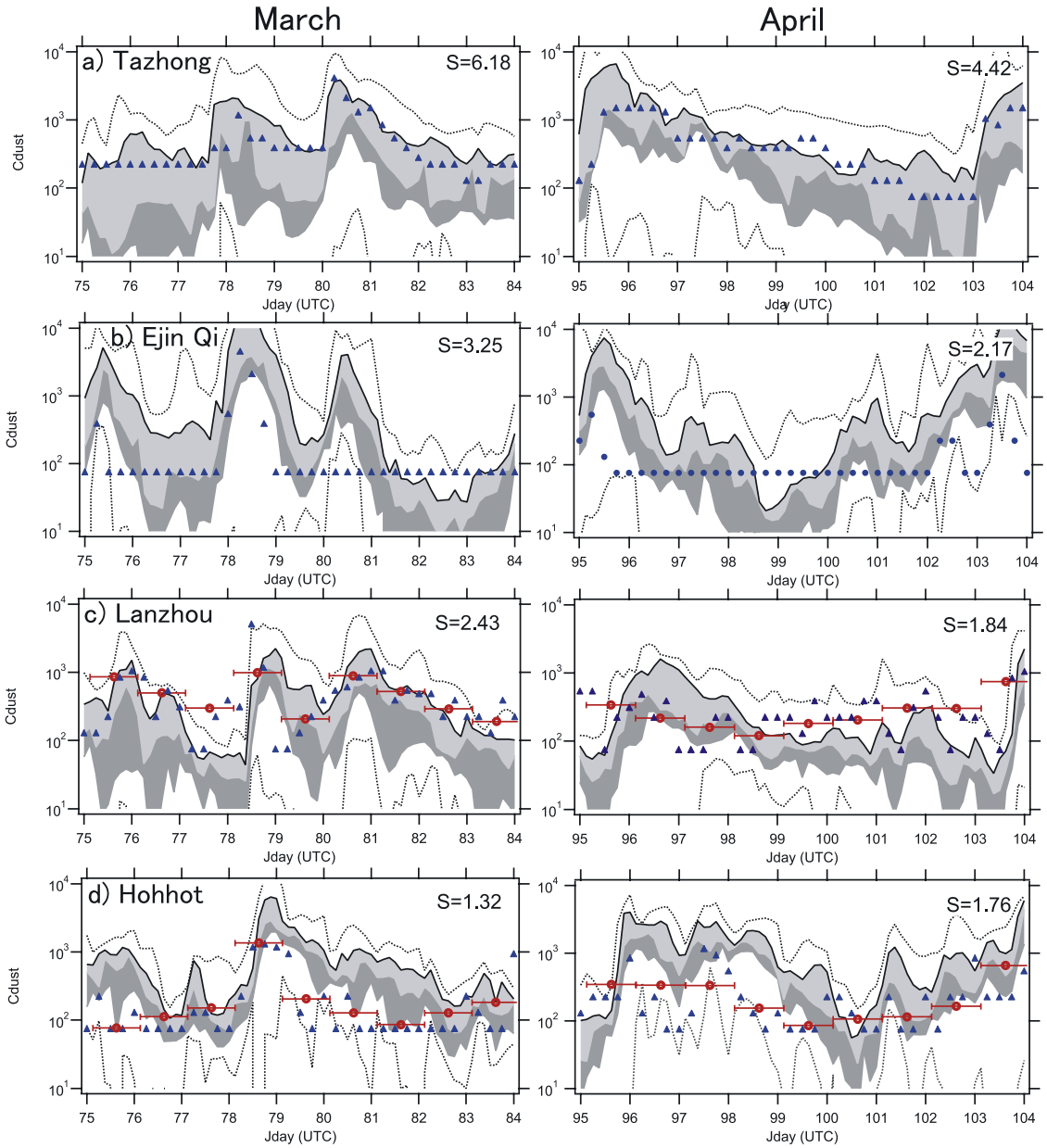

Figure 7. Time variation of the surface dust concentration ($\mu g/m^3$). (a) Tazhong, (b) Ejin Qi, (c) Lanzhou and (d) Hohhot. The surface dust concentration from each model is shown by min, 25%, 50% (mode), 75%, and max value. Quartile value between 25% and 75% percentile are shaded. Triangles are observed VC_{TSP} converted from SYNOP visibility. The circles with horizontal bar are daily averaged PM_{10} measurements from the Chinese SEPA sites.

[19] The model results have scatter with a large deviation. There was no systematic difference between the high-resolution and low-resolution horizontal grid model groups (not shown in Figure 6). A great difference was revealed in the Tazhong site (the center of the Taklimakan Desert), whereas the wind speed difference in Ejin Qi (located in the Gobi Desert) was relatively small. At Hohhot, all model results overestimated the wind speed, but they captured the day-to-day variations quite well. One reason for this systematic difference might be the site location. Hohhot is located within a relatively steep valley. Therefore there could be a difference in elevation between the observation site and the model grid point. The observed wind speeds at Beijing and Taiyuan are sometimes higher than the maximum of the modeled values, but the reason is not certain at this moment. Nevertheless, it is clear that modeled range of $WS_{25\%}-WS_{75\%}$ percentiles generally reproduce the observed wind variation.

[20] It is important to mention here that all DMIP dust models are based on the output of global or regional meteorological models using objective analysis results (such as NCEP, ECMWF, JMA, and NOGAPS); in addition, the horizontal resolution of models is 27–100 km. This resolution can be considered as high, and topographical resolution might not exert a great difference among the models. It was also found that the highest-resolution model is not

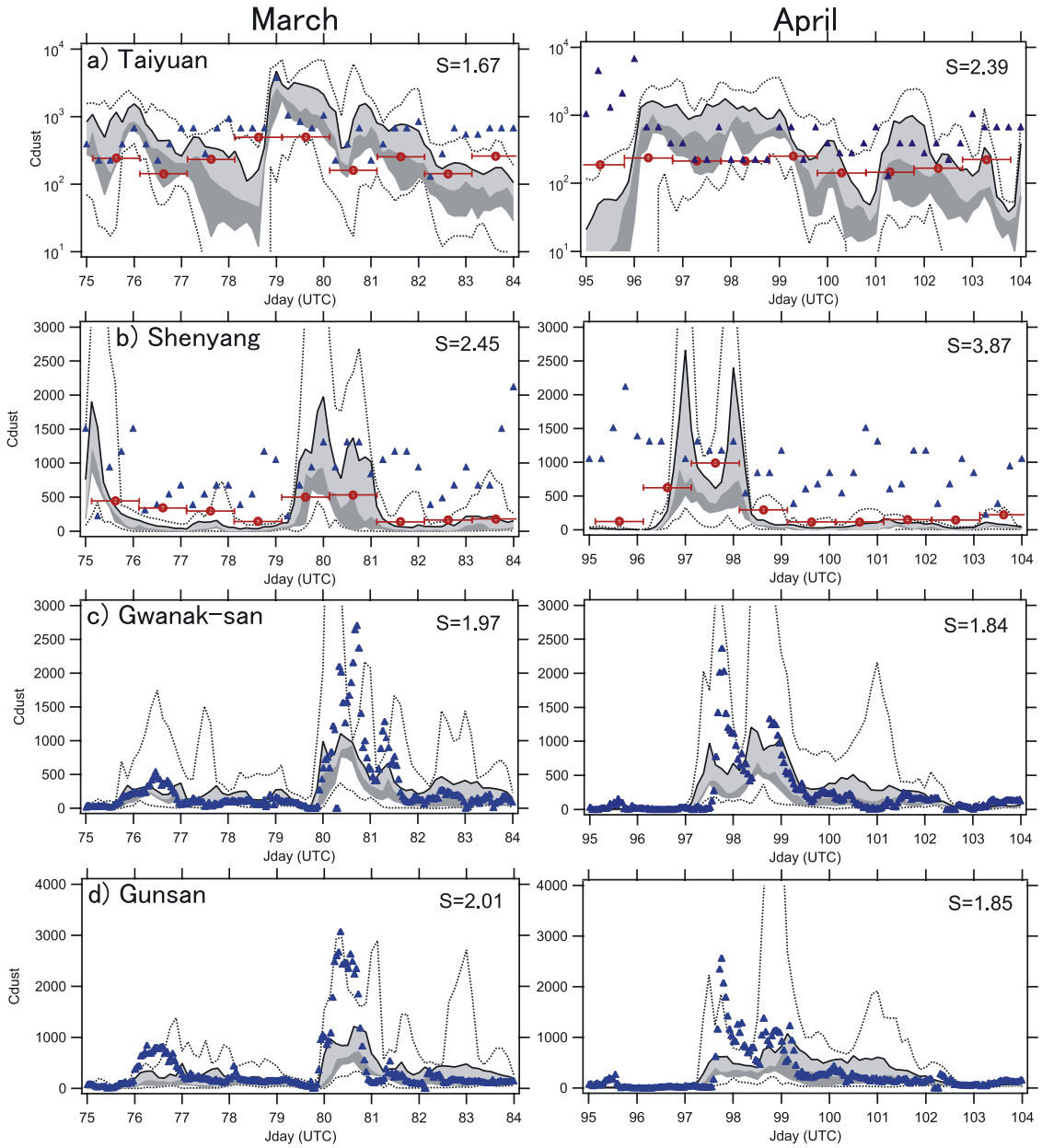

Figure 8. Time variation of the surface dust concentration (μg/m^3). (a) Taiyuan, (b) Shenyang, (c) Gwanak-san and (d) Gunsan. The surface dust concentration from each model is shown by min, 25%, 50% (mode), 75%, and max value. Quartile value between 25% and 75% percentile are shaded. Triangles in Figures 8a and 8b are observed VC_{TSP} converted from SYNOP visibility. The circles with horizontal bar (Figures 8a and 8b) are daily averaged PM_{10} measurements from the Chinese SEPA sites. Gwanak-san and Gunsan (Figures 8c and 8d) are TSP from the Korean Meteorological Administration.

always that which best fits the observations (not shown in Figure 6). The dust emission flux is fundamentally proportional to the third or fourth power of the surface friction velocity (u_*). Therefore even small differences (say, 2–3 m/s) will engender a factor of 2 or 3 times difference in dust emission flux. This fact indicates that the difference in model results may lie within the meteorological parameters. Improvement of the meteorological model is a key issue to reduce the differences among dust models.

[21] The meteorological fields from the various models differ, significantly at times, as was shown in Figure 6, thereby complicating the comparison of the dust emission. The necessity of the unified meteorological condition for dust model comparison was argued within the DMIP community. However, each dust model is strongly connected to its own meteorological driver (model) and the usage of unified meteorological conditions was considered impractical by the participating groups. Consequently, unified meteorological data were not specified for the DMIP groups. Further statistical analyses and discussion of the wind fields are presented in section 4.4.

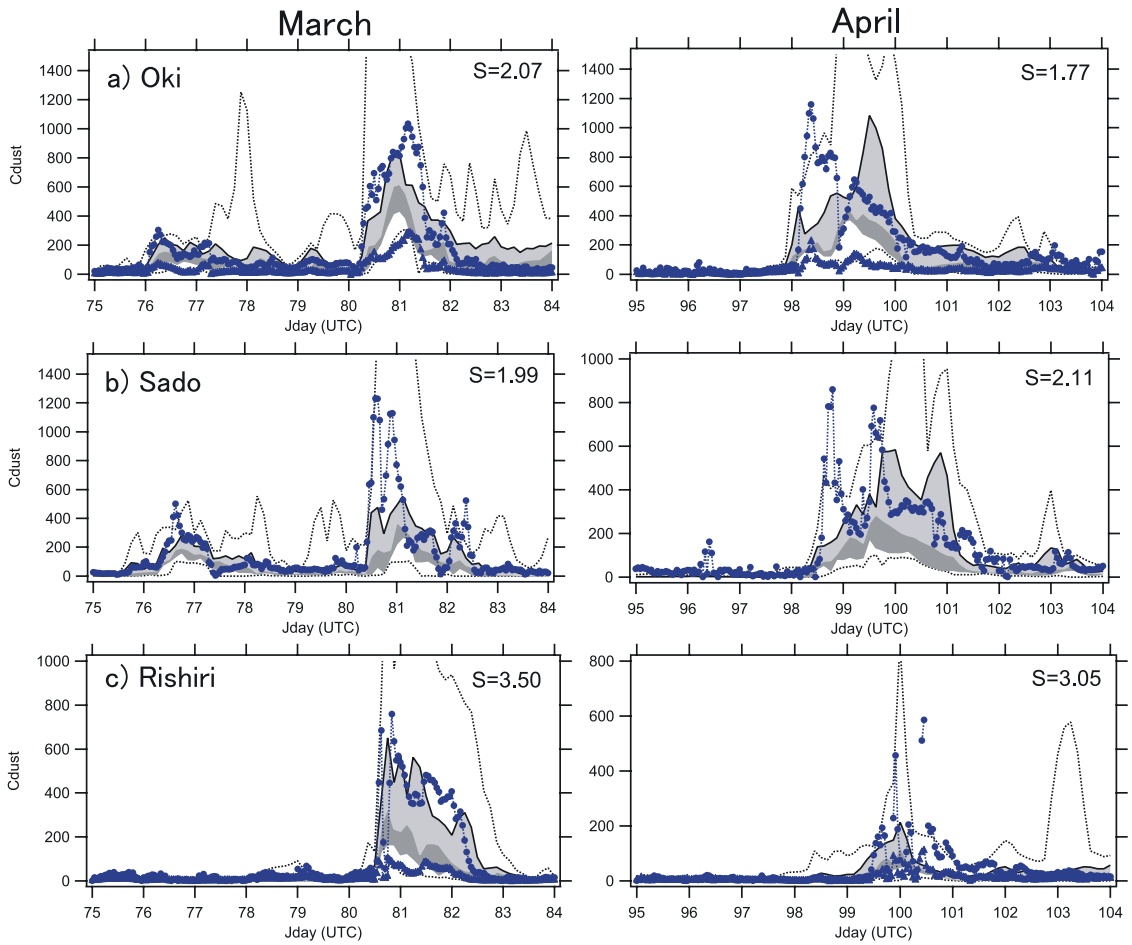

Figure 9. Time variation of the surface dust concentration (μg/m^3). Sites are Oki, Sado, and Rishiri. The surface dust concentration from each model is shown by min, 25%, 50% (mode), 75%, and max value. Quartile value between 25% and 75% percentile are shaded. Triangles are observed PM_{10}, and circles are $PM_{2.5}$.

4.3. Time Series Comparisons of Surface Dust Concentration

[22] Figures 7–10 show a comparison of modeled surface dust concentration with observations. Dust concentration results from China (Tazhong, Ejin Qi, Lanzhou, Hohhot, Taiyuan, Shenyang; Figures 7 and 8) are compared with the estimated TSP concentration (VC_{TSP}) and SEPA PM_{10} concentrations (daily averaged values). In Korea (Gwanaksan and Gunsan; Figure 8), the modeled dust concentrations are compared with the KMA TSP observations. In Japan (Oki, Sado and Rishiri; Figure 9) the comparison is made with the EANET PM_{10} and $PM_{2.5}$ data. Geographical locations of these observation sites are shown in Table 3 and Figure 1. As shown in Figure 6, the surface dust concentrations from each model are sorted statistically and show the minimum, quartile values (25%, 50% and 75% percentile values), and maximum concentration.

[23] It is clearly seen in Figures 7 and 8 that the modeled dust concentration captured the time variation of VC_{TSP} and SEPA PM_{10} quite well. Some models yield extremely high or low concentrations. Nevertheless, most of time, the observed values are distributed within the model range of $C_{25\%}$–$C_{75\%}$.

[24] There exists a very wide scatter of dust concentrations at Tazhong (Taklimakan Desert). Sometimes, the instantaneous value of nondimensional model variation S_{DC1B} exceeded 20. Averaged over the period A S_{DC1B} is 6.18 and period B it is 4.42, which is the highest in this comparison. Figure 7a portrays the large range of modeled dust concentrations at Tazhong, which is very reasonable because of the widely varying wind speeds. This result reinforces the importance of dynamical forcing to dust emission and transport modeling over the Taklimakan Desert, which has been pointed out by *Shao and Wang* [2003] and *Uno et al.* [2005].

[25] At Shenyang, model predicted concentrations for April agreed quite well with SEPA PM_{10} but were less than VC_{TSP} values. The good correlation between VC_{TSP} and SEPA PM_{10} at Lanzhou and Hohhot (Figures 7c and 7d) supports the validity of equation (1). The poorer correlation (with VC_{TSP} > SEPA PM_{10}) at Taiyan and Shenyang (Figures 8a and 8b) points to an increasing contribution by aerosols other than dust in visibility degradation.

[26] At Beijing (Figure 10), the time variation between VC_{TSP} and BNU_TSP value shows very good agreement (except for the absolute concentration). The models also captured this variability well. Dust extinction coefficients by

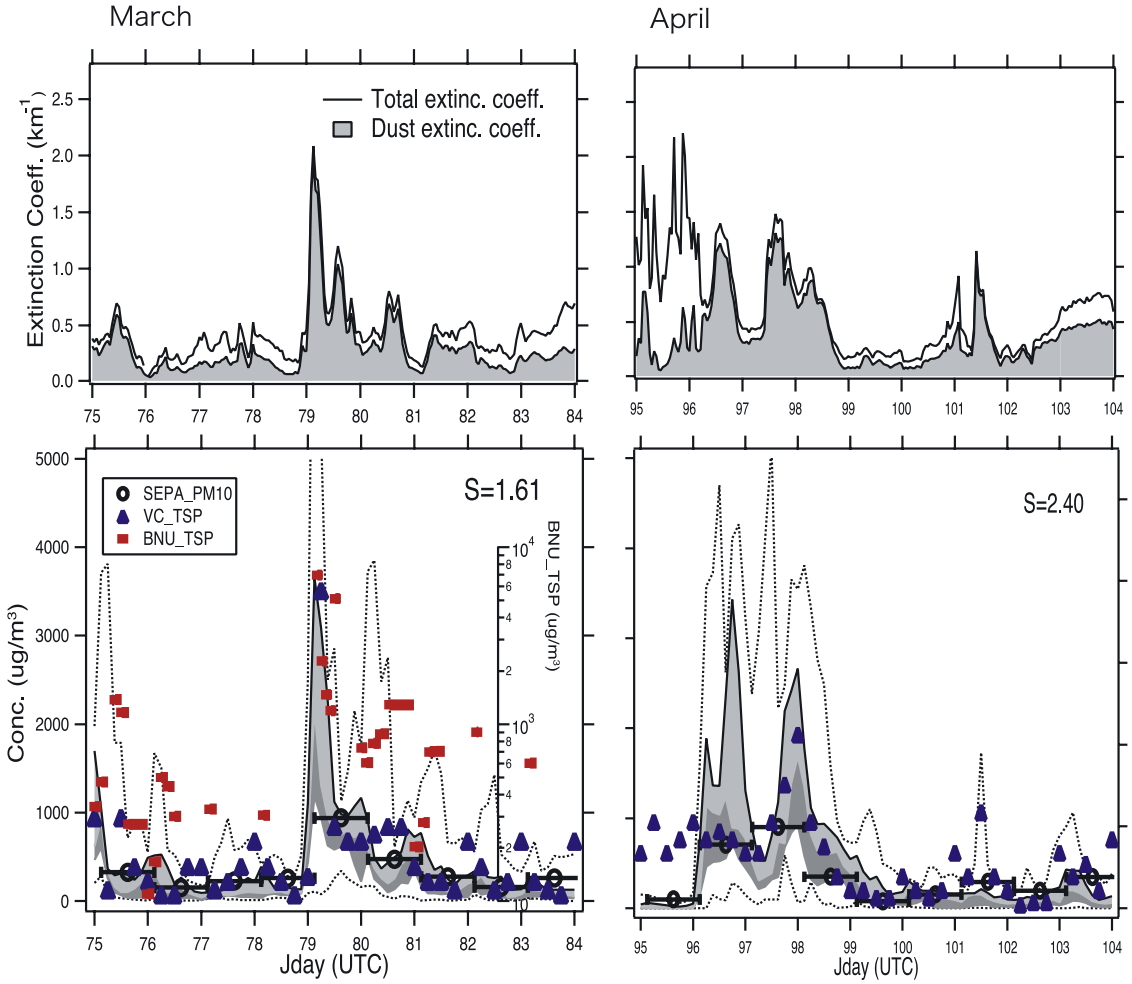

Figure 10. (top) Total and dust extinction coefficients at Beijing by NIES lidar and (bottom) model dust concentration by lines (min, 25%, 50%, 75%, and max values). The SEPA PM_{10} is shown by a black circle; BNU_TSP is represented by a red horizontal bar, and the visibility base VC_{TSP} is shown as a blue triangle.

NIES lidar also show a very sharp increase of dust extinction coefficients between Julian days 79 and 80, as simulated by the models. In March, the modeled and observed TSP (PM_{10}) concentrations had a common single peak. In April, the modeled dust concentrations showed twin peaks in China (first peak at Julian day 96 and second peak at 97–98 at Beijing), which agree well with lidar measurement. At this point, we want to point out that the greatest scatter in model dust concentration at Julian day 79 (20 March) and Julian days 96–97 (6–7 April).

[27] The TSP and PM_{10} observations in Korea and Japan (Figures 8 and 9) are also well reproduced by the DMIP models. The model variation range of $C_{25\%}$–$C_{75\%}$ shows excellent agreement with PM_{10} and TSP observations when we consider the onset timing of dust. The modeled dust concentrations in Japan (Figure 9) are usually between the observed PM_{10} and $PM_{2.5}$ values. One important point is that modeled and observed dust concentrations in Korea and Japan had a twin peak in March (around Julian days 76–77 and 80–81) except at Rishiri. We can see the similar twin peak in Ejin Qi (located in Gobi source region) and Lanzhou stations (and other stations). However, the observation of this twin dust peak strongly depend on the location of observation site and dust transport path. Another point is that the $C_{75\%}$ value shows good agreement with the Japanese PM_{10} observation (which means the averaged model concentration tends to underestimate the dust concentration in Korea and Japan).

[28] On the basis of analyses presented for Figures 7 and 10, the observed TSP and PM_{10} concentrations are generally located within the modeled $C_{25\%}$ and $C_{75\%}$ range in China, whereas $C_{75\%}$ has a better agreement in Korea and Japan. We emphasize that the model dust concentration captured the onset and cessation timing of dust phenomena well. However, the prediction of the absolute concentration level itself still presents scattering in the model output.

4.4. Area-Specified Statistics

[29] As shown in previous sections, there exists a wide range of scatter in modeled meteorological parameters and dust concentrations. The time-averaged statistics from all model outputs within the four subdomains in Figure 1 was examined. The specified areas are the Taklimakan desert (T), the Gobi desert (G), inner Mongolia (I), and southern

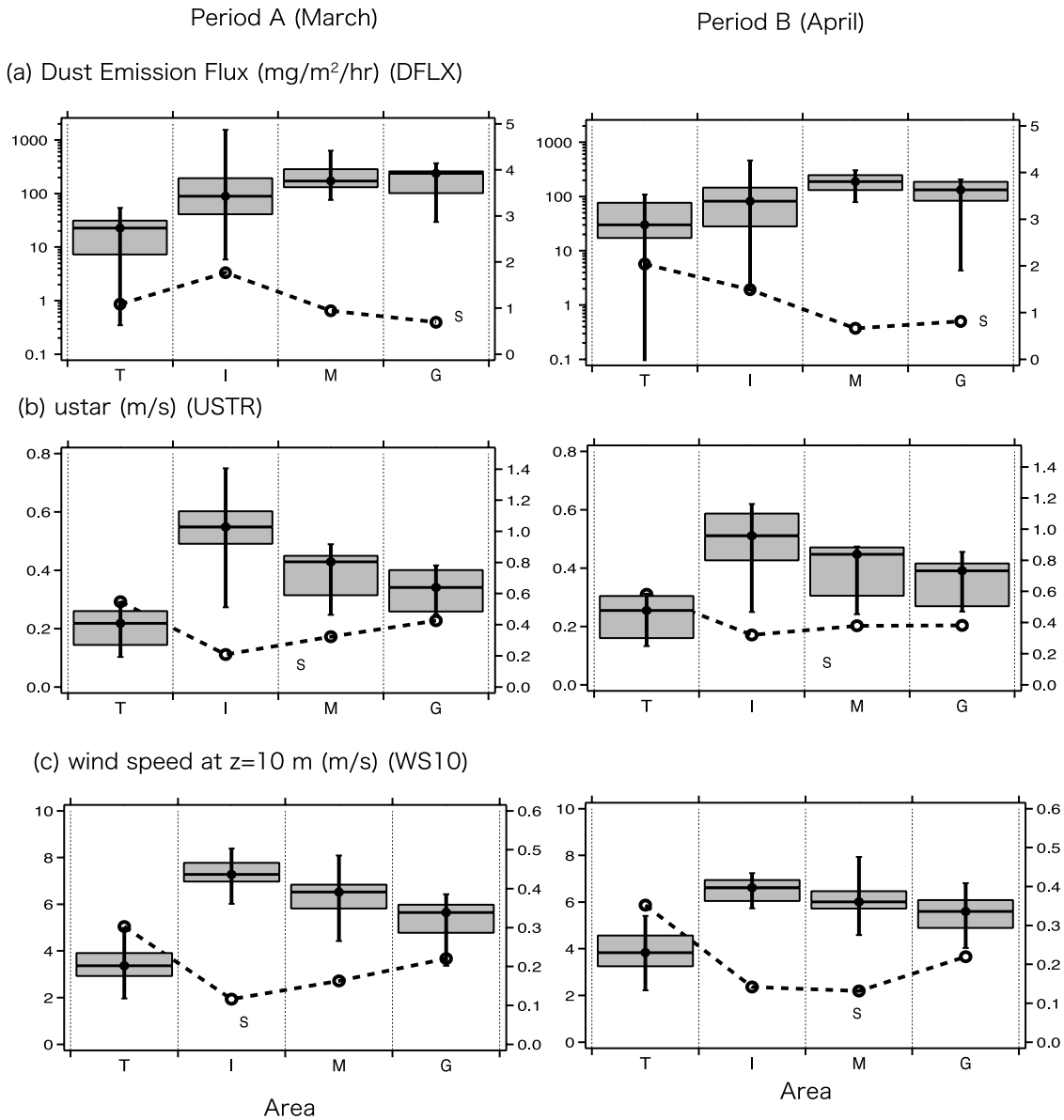

Figure 11. Area averaged (a) dust emission flux (DFLX), (b) u_* (USTR), and (c) surface wind speed at 10 m height (WS10). Averaged areas are shown in Figure 1; T (Taklimakan), I (inner Mongolia), M (Mongolia), and G (Gobi). The dashed line shows the scatter ratio S defined by equation (2). The left column is for March, and the right column is for April. Boxes represent ranges of 25% and 75% percentile values. Circles represent the 50% (mode) point, and error bars show the range of minimum and maximum.

Mongolia (M), together with several examination areas over Beijing, Qingdao, Seoul, Fukuoka, and Sado (the 2° longitude × 2° latitude area centered over each city). Table 3 lists the longitude-latitude of each area and city. Because of the large scatter in the results, the quartiled statistics were used to exclude those extreme values.

[30] A large difference is shown for DFLX (see Figure 11a). For example, over the Taklimakan area (T) in April, the averaged dust emission flux ranges from $DFLX_{25\%}$ = 16.7 to $DFLX_{75\%}$ = 78.2 mg/m^2/h with S_{DFLX} = 2.04. The averaged dust concentration ranges from $DC1B_{25\%}$ = 181 to $DC1B_{75\%}$ = 1120 μg/m^3 with S_{DC1B} = 1.83. For the Gobi area (G) in April, the dust emission flux ranges from $DFLX_{25\%}$ = 81.8 to $DFLX_{75\%}$ = 190.0 mg/m^2/h with S_{DFLX} = 0.81. The dust concentration ranges from 371 to 1848 μg/m^3 with S_{DC1B} = 1.67. The largest nondimensional scatter ratios of DFLX (S_{DFLX}) were found in areas I (inner Mongolia) and T (Taklimakan), indicating that the dust emission from these two areas differs greatly among the DMIP models. It should be noted that S_{DFLX} is greater than 0.47 in every area.

[31] Figure 12 also shows that S_{DC1B} in areas T and G have the highest values in both March and April. Ranges of concentration variation tend to decrease downwind of the sources to the down stream cities (i.e., toward Korea and Japan). Within the dust source areas of T and G, S_{DC1B} is

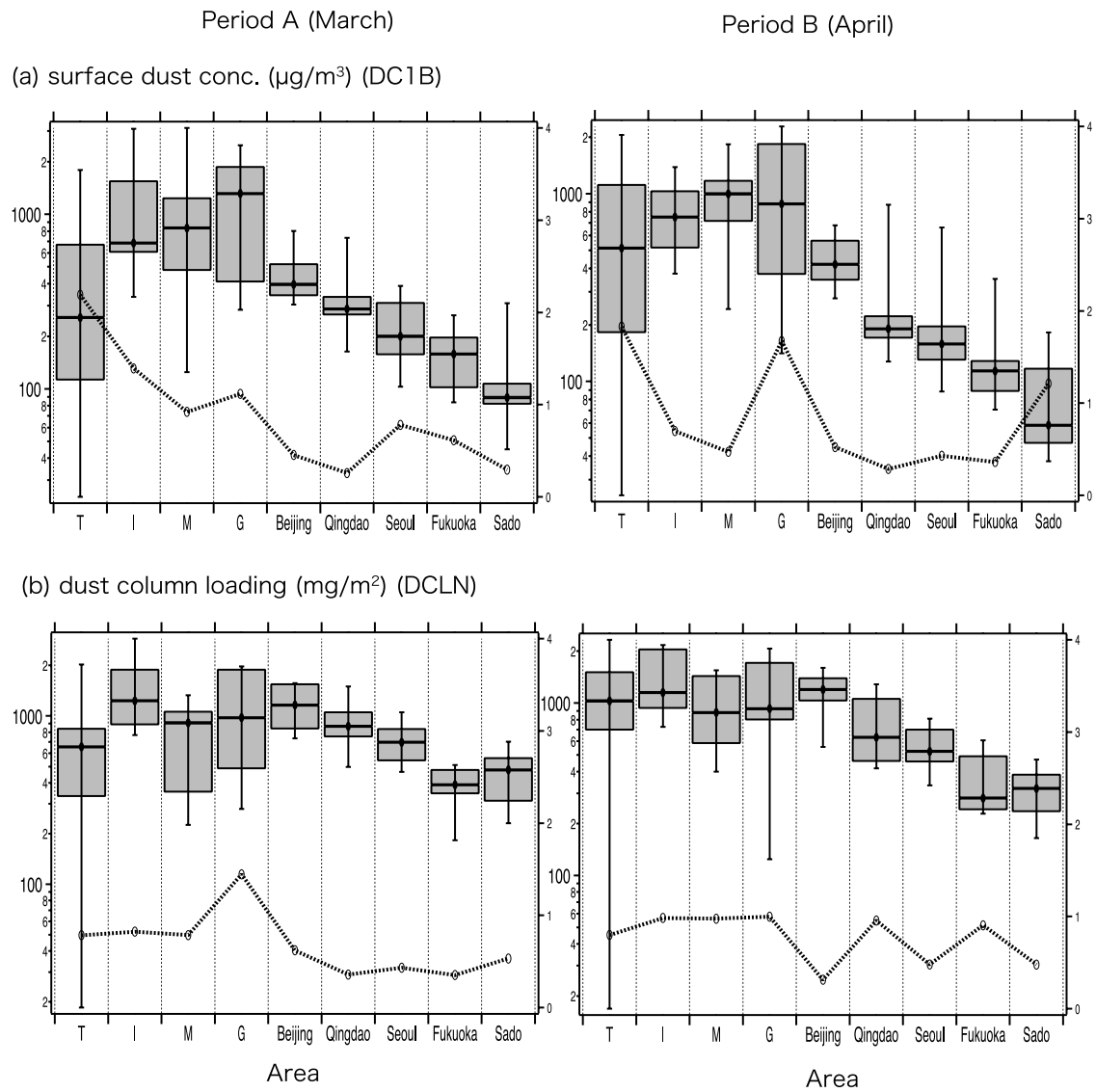

Figure 12. As in Figure 11 but for (a) surface dust concentration (DC1B) and (b) dust column loading (DCLN). The line shows the scatter ratio S defined by equation (2). The left column shows March, and the right column shows April.

always greater than 1.2 and reduces to about 0.3–0.8 downwind (except for Sado in April). These tendencies imply that the range of dust concentration differences is almost 120% of its average value within the dust source areas.

[32] Comparing Figures 12a and 12b we see that the DC1B falls off with distance from the source more quickly than DCLN owing to the fallout of large particles (the ratio between DC1B and DCLN (based on the mode value) is 1:(0.7–1) for Mongolia and Gobi, 1:1.5 for inner Mongolia, and 1:3 for other areas (not shown in Figure 12)). This pattern is quite reasonable because the dust particles over the dust source area include coarse (large) particles, which are removed by gravitational settling and other deposition processes during transport. However, the individual slope between DC1B and DCLN over the source region for each model has a wide large scatter of 1:(0.4–2), which is highly dependent on the treatment of dust emission strength and dynamical forcing.

[33] Figure 13 presents the correlation between averaged model parameters for each area and each model. In Figure 13 we show WS10 versus surface friction velocity u_*.

[34] The results shown in Figure 13 are complicated. There is a relatively clear relationship between wind speed and surface friction velocity within the DMIP group (Figure 13). Two groups can be identified in each area. For example, the model groups 3, 6 and 8 are separated from the others and take different slopes of u_* level, even for the same surface wind speed. This separation is apparent for all four areas indicating that the treatment of surface roughness length, wind shear, and surface heat flux is highly dependent on the DMIP model type. A weak positive correlation exists between WS10 and u_*, except for the Mongolia area (M).

4.5. Vertical Profile Comparisons

[35] In this section, the differences in the vertical concentration profiles is discussed. As described in section 3,

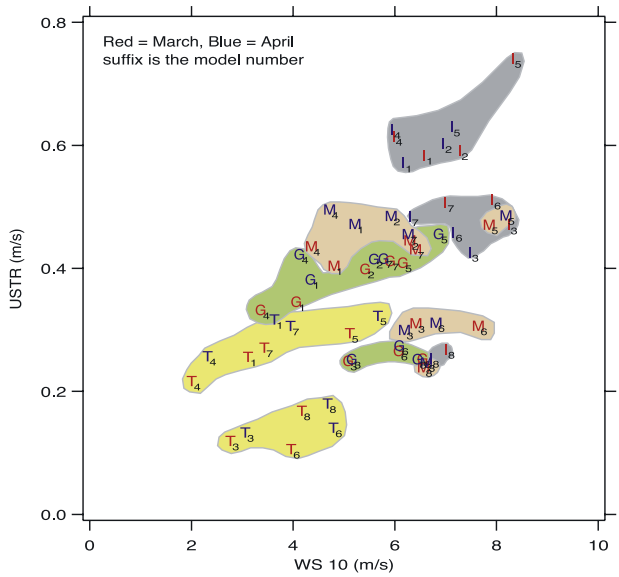

Figure 13. Scatter of area averaged surface wind speed (WS10) and u_* (USTR) averaged for 10 days. Letters indicate the area (I, M, G, and T shown in Figure 1), and the suffix shows the model number expressed anonymously by a code number. A color tone is used for each area to demarcate and clarify trends for each area and model.

NIES lidar observation results provide some verification of the model results. Beijing and Nagasaki are selected for the comparison of dust vertical profiles.

[36] Figures 14 and 15 show the time-height (TH) cross section of the potential temperature and dust concentration at Beijing (Figures 14a and 15a) and Nagasaki (Figures 14b and 15b). The NIES lidar dust extinction coefficient is also shown in Figures 14 and 15.

[37] The NIES lidar observation captured the dust onset to both Beijing and Nagasaki very clearly. Figures 2, 3, and 10 show that the big dust onset to Beijing occurred on Julian days 79–81. The lidar measurement shows that the vertical extent of this dust layer is from the surface to approximately 2 km level (i.e., most dust is captured within the boundary layer), but the highest concentration is near the surface. For Nagasaki, the lidar operation started mainly from Julian day 79. They observed the major onset of dust around Julian day 81–82 from the surface to 2 km altitude. It should be noted that lidar sometimes cannot retrieve the dust signal correctly when the dust layer is so dense to penetrate into the upper layer as pointed out by *Uno et al.* [2004].

[38] As Figure 14a shows, every model captured a large-scale dust onset in Beijing around Julian days 79–81 (shown in Figure 2). Every TH profile of dust and potential temperature appears similar. For the vertical dimension,

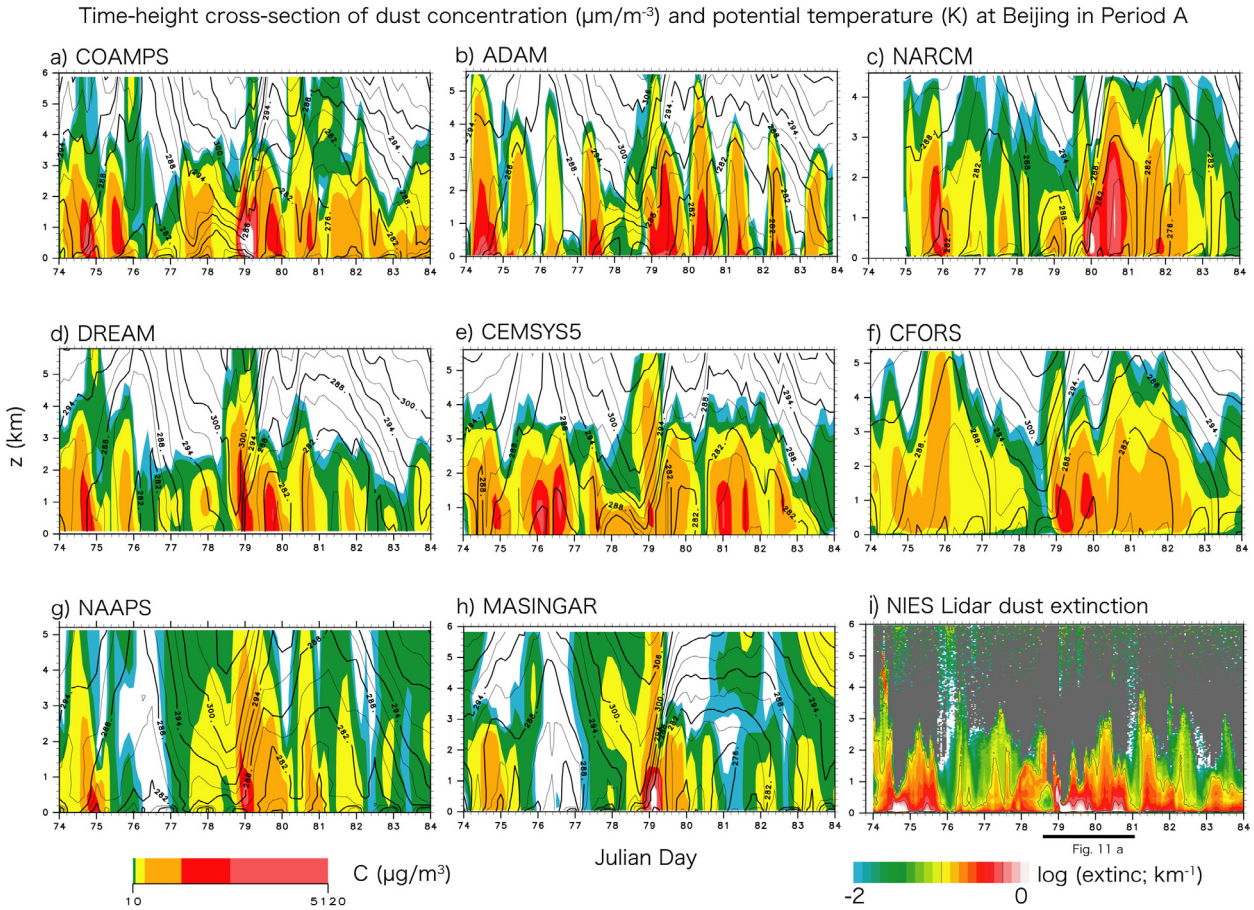

Figure 14. (a–h) Time-height cross section of dust concentration and potential temperature for each model during period A (March 2002) for Beijing, China. (i) Dust extinction coefficient by NIES Mie lidar system.

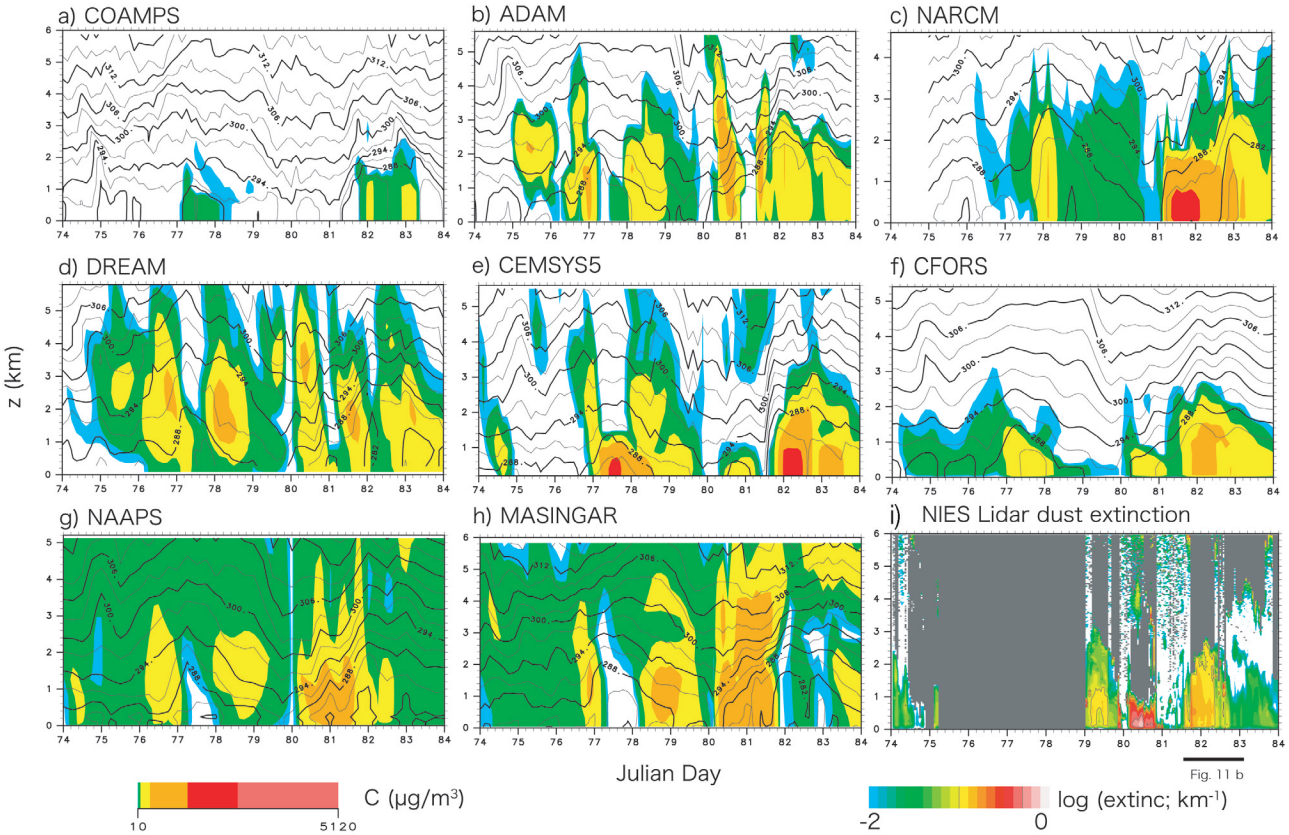

Figure 15. (a–i) As in Figure 14 but for Nagasaki, Japan.

most DMIP models reproduced the BL dust layer quite well. For Nagasaki (Figure 15b), most of the models reproduced the correct onset timing of dust that arrived around Julian days 81–82, but they show different vertical profiles and dust concentration levels. It is interesting to point out that the time-height variation of the potential temperature from the vertically high resolution model shows the fine structure (e.g., COAMPS).

[39] Figure 16 compares the time averaged vertical dust profile. Modeled dust concentrations from the typical dust episodes days are averaged and plotted in Figure 16 for Beijing (Figure 16a) and Nagasaki (Figure 16b). As in Figure 6, modeled results are sorted to show the quartiled values (shaded zone is the range of 25% and 75% percentiled value). The small figure inserted in the upper right section shows the scaled dust profile (C_*) by column dust loading (height below H = 10 km). The NIES lidar dust extinction coefficient is also time averaged and shown in Figure 16 (dashed line).

[40] Beijing (Figure 16a) shows a wide scatter of dust concentration level of each model (S_C is larger than 0.35), which is mainly attributable to the difference of dust concentration level, as shown in Figure 12. However, the shapes of the scaled dust concentration profiles have similar profiles, indicating that the main body of dust concentration is captured within the BL for both March and April episodes. It is important to point out that boundary dust layer in Beijing is so dense that the vertical profile by lidar dust tends to underestimate the upper level dust profile, and this may be a reason for the difference between lidar and dust models.

[41] At Nagasaki (Figure 16b), the vertical dust profiles differ greatly among models (even after by scaling). Some models show an elevated dust peak and others show a surface layer peak. The nondimensional scatter ratio S, as defined by equation (2), was also calculated. The S value for dust concentration below 2 km is greater than 0.35 for Beijing and greater than 1.0 for Nagasaki, which indicates that Nagasaki has a much larger scatter among the DMIP models. This suggests that modeled dust transport/removal processes between China and Japan must be an important issue in improving the dust modeling. Furthermore, it is important to correct transport and removal processes after the dust departs the continent.

5. Concluding Remarks

[42] A dust model intercomparison project (DMIP) over Asia with eight dust emission/transport models has been accomplished. Two large dust episodes occurred in spring 2002 and were used as the focus for the DMIP study. The submitted model results of DMIP are all based on the original dust emission, transport, and deposition schemes, and have a wide variety of dust emission distribution, surface concentration, and transport processes. Each model has a different dust size bin range and horizontal grid resolution. The meteorological parameters, dust emission flux, and concentration ($d < 20\ \mu m$) are compared within the same domain. The major findings from this DMIP activity can be summarized as follows:

[43] 1. The modeled surface dust concentrations are compared with SYNOP visibility, Chinese SEPA PM_{10},

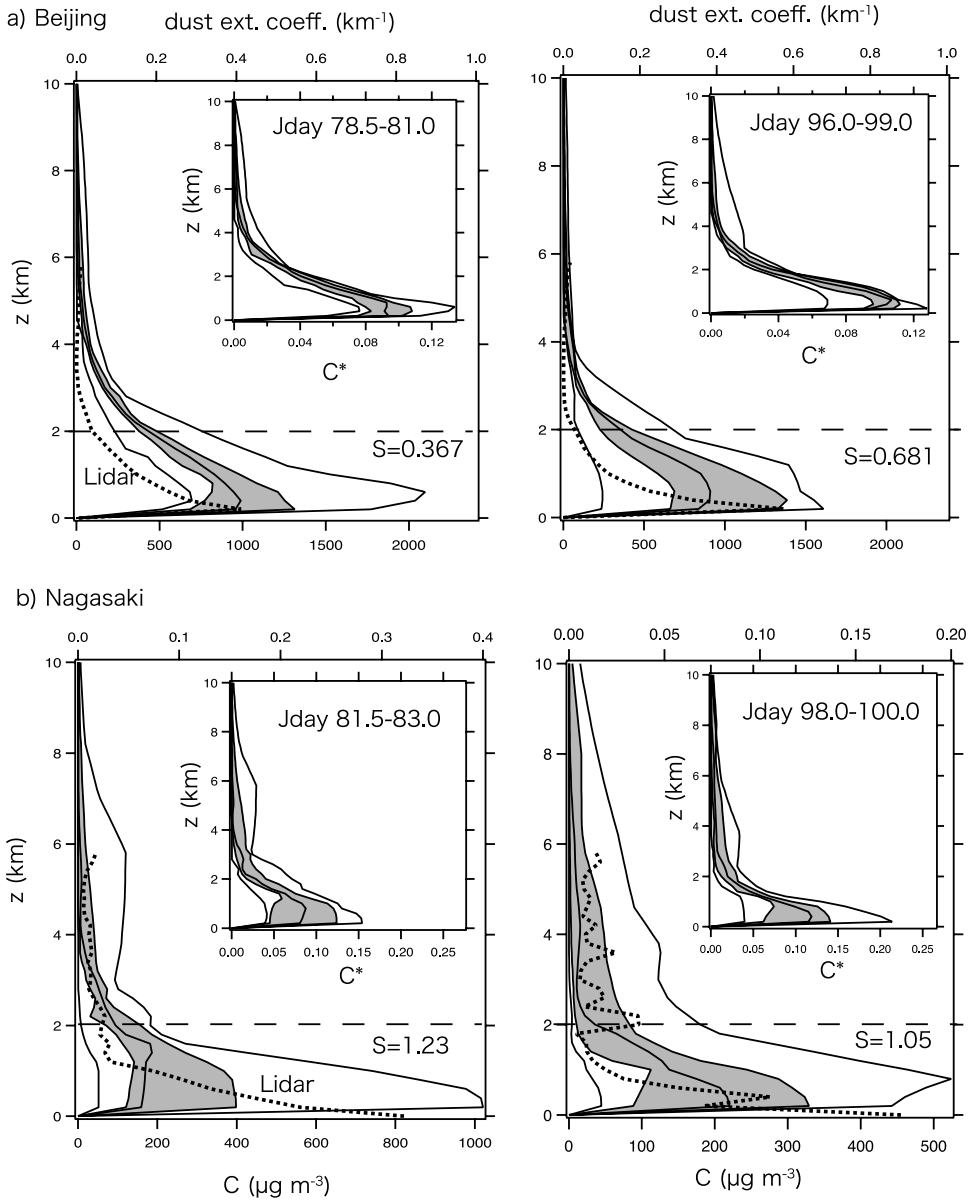

Figure 16. Averaged vertical dust profile at (a) Beijing and (b) Nagasaki. The inset is the scaled dust concentration by dust column loading (below height 10 km). The dashed line is dust extinction by NIES Mie lidar (upper scale). The shaded region is $C_{25\%}$–$C_{75\%}$ of the model output.

Korean KMA TSP, and Japanese EANET PM_{10} concentrations at several sites. It is found that a modeled concentration ranging between 25% and 75% percentile generally agreed with PM observation. The model results correctly captured the major dust onset and cessation timing at each observation site. However, the peak concentration level of each model was 2–4 times different.

[44] 2. The dust concentration during the major dust onsets shows a quite similar distribution, except for its concentration level. However, the averaged dust emission flux and wind field show visible differences. In particular, the dust emission fluxes from the Taklimakan Desert and Mongolia differ immensely among the models, indicating that the possible dust source allocation scheme and modeled winds over these regions differ greatly by each modeling group. Measurement of surface winds, dust flux and accurate or updated land use information are important in these regions.

[45] 3. The regional averaged statistical analyses clearly indicate that (1) meteorological parameters (wind speed and friction velocity) over the Taklimakan area are highly uncertain, (2) the dust emission flux from inner Mongolia has the greatest scatter, and (3) surface dust concentrations over Mongolia and Gobi have large scatter. The differences decrease downwind over Korea and Japan, even though the nondimensional scattering ratio (equation (2)) is larger among the model results. This reduced discrepancy means that the influence of the difference in dust emissions over the source area diminishes during long-range transport.

[46] 4. The comparison of the dust vertical concentration profile of Beijing and Nagasaki show large scatter (more than twice the scatter in concentration level). For Beijing,

the scaled dust profile has a similar vertical profile and relatively good agreement with the lidar extinction profile. For Nagasaki, the scaled dust profile did not have a single profile, indicating that modeled dust transport/removal processes between China and Japan is an important issue in improving the dust modeling. It is important to correctly model transport and removal processes after the dust clouds depart the continent.

[47] Results of the current DMIP project provide several important directions for the future study of Asian dust modeling and observations. Here we want to point out several directions: (1) further study of dust emission and transport from the Taklimakan Desert is important; (2) dust emissions from Mongolia and inner Mongolia have been only sparsely measured and are highly model-dependent and require more observations and consensus within the dust modeling community; and (3) statistical analyses demonstrate that the scatter of dust concentration among the different dust models diminishes after long-range transport. This last point implies that measurement near the source region is more important, especially for the dust emission flux, dust size distribution, and vertical profile.

[48] Numerical dust forecast are now operationally used in JMA (Japan Met. Agency) and KMA (Korean Met. Agency), however, their forecast accuracies depend on several conditions. This is because the dust emission processes are sometimes not properly forecasted (or identified). At this moment, as shown in this paper, reliable surface land use conditions and soil/surface information are more important than the complexity of the dust emission scheme or model horizontal resolution. While the accurate information over the desert area in China and Mongolia is very important, the availability of most updated Chinese/Mongolia databases depends on the modeling group's interest and connection. Despite these differences, most of the observed dust concentrations are within the 25–75% percentile of model forecasts. We conclude that an operational ensemble dust forecast, made up of the different numerical models based on the several sources of land use and soil information, dust emission schemes and meteorological model outputs, would provide useful forecasts of dusty weather.

[49] **Acknowledgments.** This work was performed through the project work of Aeolian Dust Experiment on Climate Impact (ADEC) supported by the Ministry of Education, Culture, Sports, Science and Technology of Japan and National Natural Science Foundation of China (project 40305018). The authors wish to acknowledge the Chinese Meteorological Agency (CMA) for their preparation of the SYNOP data set used in this study and Yasunori Kurosaki of the Meteorological Research Institute (currently at Center for Environmental Remote Sensing, Chiba University) for his analyses of SYNOP observation data. We would also like to acknowledge the Chinese SEPA for their PM_{10} measurement, Beijing Normal University for PM_{10} and TSP, KMA for their TSP, and EANET for PM_{10} data for the use of model comparison.

References

Alfaro, S. C., A. Gaudichet, L. Gomes, and M. Maille (1997), Modeling the size distribution of a soil aerosol produced by sandblasting, *J. Geophys. Res.*, *102*, 11,239–11,249.

Chin, M., P. Ginoux, R. Lucchesi, B. Huebert, R. Weber, T. Anderson, S. Masonis, B. Blomquist, A. Bandy, and D. Thornton (2003), A global aerosol model forecast for the ACE-Asia field experiment, *J. Geophys. Res.*, *108*(D23), 8654, doi:10.1029/2003JD003642.

Chinese Academy of Sciences (1998), Chinese desertification map, Resource and Environment Database, Beijing.

Christensen, J. H. (1997), The Danish eulerian hemispheric model—A three-dimensional air pollution model used for the Arctic, *Atmos. Environ.*, *31*, 4169–4191.

Chun, Y., and J.-Y. Lim (2004), The recent characteristics of Asian dust and haze events in Seoul, Korea, *Meteorol. Atmos. Phys.*, *87*, 143–152.

DeFries, R. S., and J. R. G. Townshend (1994), NDVI-derived land cover classification at a global scale, *Int. J. Remote Sens.*, *15*(17), 3567–3586.

Gillette, D. A., and R. Passi (1988), Modeling dust emission caused by wind erosion, *J. Geophys. Res.*, *93*, 14,233–14,242.

Gong, S. L., X. Y. Zhang, T. L. Zhao, I. G. McKendry, D. A. Jaffe, and N. M. Lu (2003), Characterization of soil dust aerosol in China and its transport and distribution during 2001 ACE-Asia: 2. Model simulation and validation, *J. Geophys. Res.*, *108*(D9), 4262, doi:10.1029/2002JD002633.

Huebert, B. J., T. Bates, P. B. Russell, G. Shi, Y. J. Kim, K. Kawamura, G. Carmichael, and T. Nakajima (2003), An overview of ACE-Asia: Strategies for quantifying the relationships between Asian aerosols and their climatic impacts, *J. Geophys. Res.*, *108*(D23), 8633, doi:10.1029/2003JD003550.

In, H.-J., and S.-U. Park (2003), A simulation of long-range transport of yellow sand observed in April 1998 in Korea, *Atmos. Environ.*, *36*, 4625–4636.

Liu, M., D. L. Westphal, S. Wang, A. Shimizu, N. Sugimoto, J. Zhou, and Y. Chen (2003), A high-resolution numerical study of the Asian dust storms of April 2001, *J. Geophys. Res.*, *108*(D23), 8653, doi:10.1029/2002JD003178.

Marticorena, B., and G. Bergametti (1995), Modeling the atmospheric dust cycle: 1. Design of a soil-derived emission scheme, *J. Geophys. Res.*, *100*, 16,415–16,430.

Marticorena, B., G. Bergametti, B. Aumont, Y. Callot, C. N'Doume, and M. Legrand (1997), Modeling the atmospheric dust cycle: 2. Simulation of Saharan dust sources, *J. Geophys. Res.*, *102*, 4387–4404.

Mikami, M., et al. (2002), The impact of Aeolian dust in climate: Sino-Japanese Cooperative Project ADEC, *J. Arid Land Stud.*, *11*, 211–222.

Mikami, M., et al. (2006), Aeolian dust experiment on climate impact: An overview of Japan-Sino Joint Project ADEC, *Global Planet. Change*, in press.

Network Center for EANET (2003), Data report on the acid deposition in the East Asian region 2002, Niigata, Japan.

Nickling, W. G., and J. A. Gillies (1993), Dust emission and transport in Mali, West Africa, *Sedimentology*, *40*, 859–868.

Nickovic, S., G. Kallos, A. Papadopoulos, and O. Kalaliagou (2001), A model for prediction of desert dust cycle in the atmosphere, *J. Geophys. Res.*, *106*, 18,113–18,129.

Park, S., and H. In (2003), Parameterization of dust emission for the simulation of the yellow sand (Asian dust) event observed in March 2002 in Korea, *J. Geophys. Res.*, *108*(D19), 4618, doi:10.1029/2003JD003484.

Pielke, R. A. (1984), *Mesoscale Meteorological Modeling*, Elsevier, New York.

Shao, Y. (2001), A model for mineral dust emission, *J. Geophys. Res.*, *106*, 20,239–20,254.

Shao, Y., and H. Lu (2000), A simple expression for wind erosion threshold friction velocity, *J. Geophys. Res.*, *105*, 22,437–22,443.

Shao, Y., and J. Wang (2003), A climatology of Northeast Asian dust events, *Meteorol. Z.*, *12*, 187–196.

Shao, Y., M. R. Raupach, and P. A. Findlater (1993), The effect of saltation bombardment on the entrainment of dust by wind, *J. Geophys. Res.*, *98*, 12,719–12,726.

Shao, Y., M. R. Raupach, and J. F. Leys (1996), A model for predicting Aeolian sand drift and dust entrainment on scales from paddock to region, *Aust. J. Soil Res.*, *34*, 309–342.

Shao, Y., E. Jung, and L. M. Leslie (2002), Numerical prediction of northeast Asian dust storms using an integrated wind erosion modeling system, *J. Geophys. Res.*, *107*(D24), 4814, doi:10.1029/2001JD001493.

Shao, Y., et al. (2003), Northeast Asian dust storms: Real-time numerical prediction and validation, *J. Geophys. Res.*, *108*(D22), 4691, doi:10.1029/2003JD003667.

Shimizu, A., N. Sugimoto, I. Matsui, K. Arao, I. Uno, T. Murayama, N. Kagawa, and K. Aoki (2004), Continuous observations of Asian dust and other aerosols by dual-polarization lidars in China and Japan during ACE-Asia, *J. Geophys. Res.*, *109*, D19S17, doi:10.1029/2002JD003253.

Sugimoto, N., I. Uno, M. Nishikawa, A. Shimizu, I. Matsui, X. Dong, Y. Chen, and H. Quan (2003), Record heavy Asian dust in Beijing in 2002: Observations and model analysis of recent events, *Geophys. Res. Lett.*, *30*(12), 1640, doi:10.1029/2002GL016349.

Sun, Y., G. Zhuang, H. Yun, X. Zhang, and J. Guo (2004), Characteristics and sources of 2002 super dust storm in Beijing, *China Sci. Bul.*, *49*(8), 698–705.

Tanaka, T. Y., and M. Chiba (2005), Global simulation of dust aerosol with a chemical transport model, MASINGAR, *J. Meteorol. Soc. Jpn.*, *83A*, 255–278.

Uno, I., H. Amano, S. Emori, K. Kinoshita, I. Matsui, and N. Sugimoto (2001), Trans-Pacific yellow sand transport observed in April 1998: A numerical simulation, *J. Geophys. Res.*, *106*, 18,331–18,344.

Uno, I., et al. (2003), Regional chemical weather forecasting system CFORS: Model descriptions and analysis of surface observations at Japanese island stations during the ACE-Asia experiment, *J. Geophys. Res.*, *108*(D23), 8668, doi:10.1029/2002JD002845.

Uno, I., et al. (2004), Numerical study of Asian dust transport during the springtime of 2001 simulated with the Chemical Weather Forecasting System (CFORS) model, *J. Geophys. Res.*, *109*, D19S24, doi:10.1029/2003JD004222.

Uno, I., K. Harada, S. Satake, Y. Hara, and Z. Wang (2005), Meteorological Characteristics and dust distribution of the Tarim Basin simulated by the nesting RAMS/CFORS dust model, *J. Meteorol. Soc. Jpn.*, *83A*, 219–239.

Wang, Z., H. Ueda, and M. Huang (2000), A deflation module for use in modeling long-range transport of yellow sand over East Asia, *J. Geophys. Res.*, *105*, 26,947–26,960.

Webb, R. W., C. E. Rosenzweig, and E. R. Levine (2000), Global soil texture and derived water-holding capacities (Webb et al.) data set, http://www.daac.ornl.gov, Oak Ridge Natl. Lab. Distrib. Active Arch. Cent., Oak Ridge, Tenn.

Westphal, D. L., O. B. Toon, and T. N. Carlson (1987), A two-dimensional numerical investigation of the dynamics and microphysics of Sahara dust storm, *J. Geophys. Res.*, *92*, 3027–3049.

Westphal, D. L., O. B. Toon, and T. N. Carlson (1988), A case study of mobilization and transport of Sahara dust, *J. Atmos. Sci.*, *45*, 2145–2175.

M. Chiba, M. Mikami, and T. Tanaka, Meteorological Research Institute, Tsukuba, Ibaraki 305-0052, Japan. (mchiba@mri-jma.go.jp; mmikami@mri-jma.go.jp; yatanaka@mri-jma.go.jp)

Y. S. Chun and S.-S. Lee, Meteorological Research Institute, Korean Meteorological Administration, Seoul 156-720, Korea. (yschun@metri.re.kr; leess@metri.re.kr)

S. L. Gong, Air Quality Research Branch, Meteorological Service of Canada, Toronto, ON, Canada M3H 5T4. (sunling.gong@ec.gc.ca)

Y. Hara and I. Uno, Research Institute for Applied Mechanics, Kyushu University, Kasuga 816-8580, Japan. (yhara@riam.kyushu-u.ac.jp; iuno@riam.kyushu-u.ac.jp)

E. Jung, Center for Atmospheric Sciences, Scripps Institution of Oceanography, 9500 Gilman Drive 0221, La Jolla, CA 92093-0221, USA. (eunjoo@fiji.ucsd.edu)

M. Liu and D. L. Westphal, Naval Research Laboratory, Monterey, CA 93943, USA. (liu@nrlmry.navy.mil; westphal@nrlmry.navy.mil)

S. Music, Euro-Mediterranean Centre on Insular Coastal Dynamics, University of Malta, Foundation for International Studies, VLT07 Valletta, Malta. (s.music@icod.org.mt)

S. Nickovic, Environment Division, Atmospheric Research and Environment Program, World Meteorological Organization, CH-1211 Geneva, Switzerland. (snickovic@wmo.int)

S. Satake, Research Institute for Humanity and Nature, Kyoto 602-0878, Japan. (satake@chikyu.ac.jp)

Y. Shao, Department of Physics and Materials, City University of Hong Kong, 83 Tat Chee Agenue, Kowloon, Hong Kong. (apyshao@cityu.edu.hk)

Z. Song, National Meteorological Centre, China Meteorological Administration, 46# Zhong Guancun South Street, 100081 Beijing, China. (songzhenxin@vip.sina.com)

N. Sugimoto, National Institute for Environmental Studies, Tsukuba, Ibaraki 305-8506, Japan. (nsugimot@nies.go.jp)

Z. Wang, LAPC/NZC, Institute of Atmospheric Physics, Chinese Academy of Sciences, Beijing, 100029, China. (zifawang@mail.iap.ac.cn)